ความเข้ากันได้เชิงเคมีของแลนทานัมสทรอนเชียมโคบอลต์อะลูมิเนียมออกไซด์
ชนิดใหม่กับอิตเทรียสเทบิไลซ์เซอร์โคเนีย
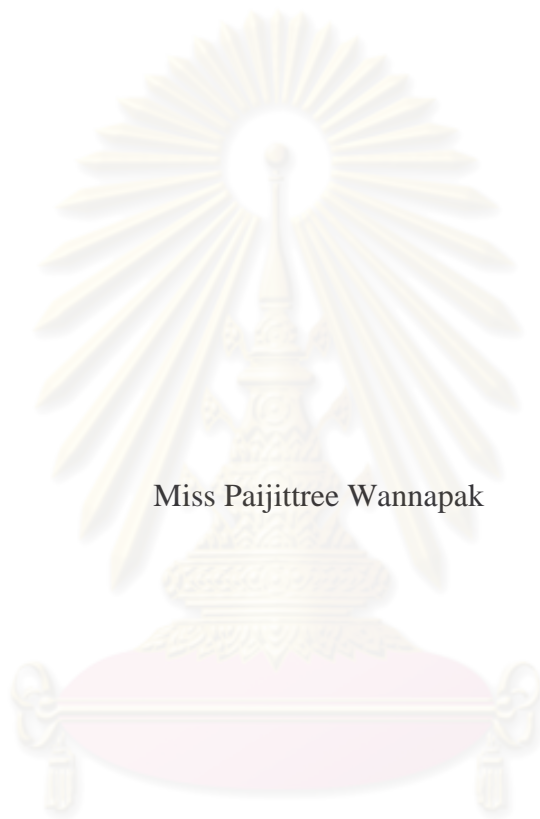
นางสาวไพจิตรี วรรณภาค

วิทยานิพนธ์นี้เป็นส่วนหนึ่งของการศึกษาตามหลักสูตรปริญญาวิทยาศาสตรมหาบัณฑิต
สาขาวิชาปิโตรเคมีและวิทยาศาสตร์พอลิเมอร์
คณะวิทยาศาสตร์ จุฬาลงกรณ์มหาวิทยาลัย
ปีการศึกษา 2552
ลิขสิทธิ์ของจุฬาลงกรณ์มหาวิทยาลัย

CHEMICAL COMPATIBILITY OF NEW LANTHANUM STRONTIUM COBALT
ALUMINIUM OXIDES AND YTTRIA STABILIZED ZIRCONIA

Miss Paijittree Wannapak

ศูนย์วิทยทรัพยากร
จุฬาลงกรณ์มหาวิทยาลัย

A Thesis Submitted in Partial Fulfillment of the Requirements

for the Degree of Master of Science Program in Petrochemistry and Polymer Science

Faculty of Science

Chulalongkorn University

Academic Year 2009

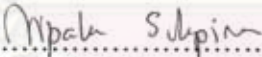Thesis Title   CHEMICAL COMPATIBILITY OF NEW LANTHANUM
                     STRONTIUM COBALT ALUMINIUM OXIDES AND
                     YTTRIA STABILIZED ZIRCONIA
By   Miss Paijittree Wannapak
Field of Study   Petrochemistry and Polymer Science
Thesis Advisor   Nipaka Sukpirom, Ph.D.
Thesis Co-Advisor   Assistant Professor Jinda Yeyongchaiwat, Ph.D.
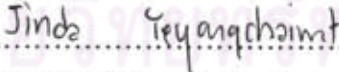
Accepted by the Faculty of Science, Chulalongkorn University in Partial Fulfillment of the Requirements for the Master's Degree

....Dean of the Faculty of Science
(Professor Supot Hannongbua, Dr. rer. nat)

THESIS COMMITTEE

....Chairman
(Professor Pattarapan Prasassarakich, Ph.D.)

....Thesis Advisor
(Nipaka Sukpirom, Ph.D.)

....Thesis Co-Advisor
(Assistant Professor Jinda Yeyongchaiwat, Ph.D.)

....Examiner
(Associate Professor Wimonrat Trakarnpruk, Ph.D.)

....External Examiner
(Watcharee Katinonkul, Ph.D.)

ไพจิตรี วรรณภาค : ความเข้ากันได้เชิงเคมีของแลนทานัมสทรอนเชียมโคบอลต์อะลูมิเนียมออกไซด์ชนิดใหม่และอิตเทรียสเทบิไลซ์เซอร์โคเนีย (CHEMICAL COMPATIBILITY OF NEW LANTHANUM STRONTIUM COBALT ALUMINIUM OXIDES AND YTTRIA STABILIZED ZIRCONIA) อ. ที่ปรึกษาวิทยานิพนธ์หลัก: ดร. นิปกา สุขภิรมย์, อ. ที่ปรึกษาวิทยานิพนธ์ร่วม: ผู้ช่วยศาสตราจารย์ ดร.จินดา ยืนยงชัยวัฒน์, 67 หน้า.

ศึกษาความเข้ากันได้เชิงเคมีของวัสดุสำหรับใช้เป็นขั้วแคโทดในเซลล์เชื้อเพลิงชนิดออกไซด์ของแข็ง คือ $La_{1-x}Sr_xCo_{1-y}Al_yO_3$ ซึ่งมีโครงสร้างแบบเพอรอฟสไกต์ และ $La_{2-x}Sr_xCo_{1-y}Al_yO_4$ ซึ่งมีโครงสร้างแบบ K_2NiF_4 กับของแข็งอิเล็กโทรไลต์ที่ใช้ในทางการค้าคือ 8 โมลเปอร์เซ็นต์ของอิตเทรียสเทบิไลซ์เซอร์โคเนีย (8-YSZ) ในขั้นแรกสารประกอบโครงสร้างแบบเพอรอฟสไกต์ที่มีสัดส่วน $0.0 < x, y < 1.0$ และโครงสร้าง K_2NiF_4 ที่มีสัดส่วน $0.0 < x < 2.0$, $0.0 \leq y \leq 1.0$ ถูกเตรียมด้วยวิธีซิเทรทประยุกต์ จากการตรวจสอบลักษณะเฉพาะด้วยเทคนิค XRD พบว่าเพอรอฟสไกต์ที่สังเคราะห์ได้และเผาที่อุณหภูมิ 900 – 1000 ℃ เป็นเวลา 5 ชั่วโมงจะได้เป็นเฟสเดี่ยวที่สัดส่วน x = 0.0 – 1.0 ยกเว้น x = 0.5 – 0.7 เมื่อ $y \leq 0.2$ และมีโครงสร้างผลึกเป็นแบบคิวบิก นอกจากนี้ค่าแลตทิช ปริมาตรต่อหน่วยยูนิตและความหนาแน่นมีแนวโน้มลดลงเมื่อเพิ่มปริมาณของอะลูมิเนียม ส่วนในกรณีของสารประกอบออกไซด์โครงสร้างแบบ K_2NiF_4 พบว่าเฉพาะสัดส่วน x = 0.8 – 1.2 ยกเว้น x = 1.1 เมื่อ y = 0.1 และสัดส่วน x = 1.0 เมื่อ y = 0.0 – 0.6 หลังจากเผาที่อุณหภูมิ 900 – 1100 ℃ เท่านั้นที่ได้เป็นเฟสเดี่ยว โดยมีโครงสร้างผลึกเป็นแบบเททระโกนัล จากนั้นศึกษาติดตามความเข้ากันได้ของ $La_{0.6}Sr_{0.4}Co_{1-y}Al_yO_3$ ที่สัดส่วน y = 0.05, 0.1 และ 0.2 และ $LaSrCo_{1-y}Al_yO_4$ ที่สัดส่วน y = 0.05, 0.2, 0.4 และ 0.6 กับ 8-YSZ ด้วยเทคนิค XRD และ SEM/EDX พบว่าสารประกอบเพอรอฟสไกต์กับ 8-YSZ เข้ากันได้เชิงเคมีจนถึงอุณหภูมิ 850 ℃ ในกรณีของสารประกอบออกไซด์โครงสร้างแบบ K_2NiF_4 พบว่าสามารถเข้ากันได้เชิงเคมีกับ 8-YSZ จนถึงอุณหภูมิ 800 ℃ นอกจากนี้พบว่าค่าสัมประสิทธิ์การขยายตัวเนื่องจากความร้อนของ $La_{0.6}Sr_{0.4}Co_{1-y}Al_yO_3$ ที่สัดส่วน y = 0.0, 0.05 และ 0.2 มีค่าลดลงเมื่อเพิ่มปริมาณอะลูมิเนียม ส่วนค่าสัมประสิทธิ์การขยายตัวเนื่องจากความร้อนของ $LaSrCo_{1-y}Al_yO_4$ ที่สัดส่วน y = 0.0, 0.05 และ 0.2 มีค่าเพิ่มขึ้นเมื่อเพิ่มปริมาณอะลูมิเนียม

สาขาวิชา ปิโตรเคมีและวิทยาศาสตร์พอลิเมอร์ ลายมือชื่อนิสิต ไพจิตรี วรรณภาค

ปีการศึกษา 2552 ลายมือชื่ออ. ที่ปรึกษาวิทยานิพนธ์หลัก นิปกา สุขภิรมย์

ลายมือชื่ออ. ที่ปรึกษาวิทยานิพนธ์ร่วม จินดา ยืนยงชัยวัฒน์

5072401223: MAJOR PETROCHEMISTRY AND POLYMER SCIENCE

KEYWORDS: PEROVSKITE / K_2NiF_4-TYPED / LANTANUM STRONTIUM COBALT ALUMINIUM OXIDES / YTTRIA STABILIZED ZIRCONIA / SOLID OXIDE FUEL CELLS

PAIJITTREE WANNAPAK: CHEMICAL COMPATIBILITY OF NEW LANTANUM STRONTIUM COBALT ALUMINIUM OXIDES AND YTTRIA STABILIZED ZIRCONIA. THESIS ADVISOR: NIPAKA SUKPIROM, Ph.D., THESIS CO-ADVISOR: ASSISTANT PROFESSOR JINDA YEYONGCHAIWAT, Ph.D., 67 pp.

The chemical compatibilities of the candidates, $La_{1-x}Sr_xCo_{1-y}Al_yO_3$ perovskites and $La_{2-x}Sr_xCo_{1-y}Al_yO_4$ K_2NiF_4-typed, of cathode material for solid oxide fuel cell with the commercial solid electrolyte, 8 mol % yttria stabilized zirconia (8-YSZ), were studied. Firstly, perovskite and K_2NiF_4-typed oxides with $0.0 < x, y < 1.0$ and $0.0 < x < 2.0$, $0.0 \leq y \leq 1.0$ respectively were prepared by modified nitric citrate method, and characterized by XRD. It was found that the single-phased perovskites were synthesized successfully at $900 - 1000^\circ C$ for 5h. When x is 0.0 - 1.0 (except x = 0.5 – 0.7), $y \leq 0.2$, the crystal structure is cubic. The lattice constants, the volume per formula unit and density decrease with the increase of Al content. The single-phased K_2NiF_4-typed oxides were achieved when x = 0.8 – 1.2 (except x = 1.1), y = 0.1 and when x = 1.0, y = 0.0 – 0.6 after calcination at $900 - 1100^\circ C$. The crystal structure of K_2NiF_4-typed oxides is tetragonal. Monitored by XRD and SEM/EDX, the $La_{0.6}Sr_{0.4}Co_{1-y}Al_yO_3$ with y = 0.05, 0.1 and 0.2 and $LaSrCo_{1-y}Al_yO_4$, y = 0.05, 0.2, 0.4 and 0.6 have a good chemical compatibility with 8-YSZ from room temperature up to $850^\circ C$ and $800^\circ C$ respectively. In addition the thermal expansion coefficients of $La_{0.6}Sr_{0.4}Co_{1-y}Al_yO_3$ (y = 0.0, 0.05 and 0.2) decrease with the increase of Al content and the thermal expansion coefficients of $LaSrCo_{1-y}Al_yO_4$ (y = 0.0, 0.05 and 0.2) increase with the increase of Al content.

Field of Study Petrochemistry and Polymer Science Student's Signature Paijittree ยุทธนะพลัก

Academic year 2009 Advisor's Signature Nipaka Sukpirom

Co-Advisor's Signature Jinda Yeyongchiwat

ACKNOWLEDGEMENTS

CONTENTS

ศูนย์วิทยทรัพยากร

จุฬาลงกรณ์มหาวิทยาลัย

LIST OF TABLES

ศูนย์วิทยทรัพยากร
จุฬาลงกรณ์มหาวิทยาลัย

LIST OF FIGURES

Figure		Page

ศูนย์วิทยทรัพยากร
จุฬาลงกรณ์มหาวิทยาลัย

LIST OF ABBREVIATIONS

K	Kelvin
°C	Degree Celsius
min	Minute or minutes
μm	Micrometer
Å	Angstrom unit
XRD	X-ray diffraction
SEM	Scanning electron microscopy
SEM-EDX	Scanning electron microscopy-energy dispersive X-ray fluorescence
TEM	Transmission electron microscopy
IS	Impedance Spectroscopy
EPMA	Electron probe microanalysis
h	Hour or hours
wt %	Percent by weight
SOFCs	Solid oxide fuel cells
IT-SOFCs	Intermediate temperature of solid oxide fuel cells
MIECs	Mixed Electronic and Ionic Conductors
ABO_3	Perovskite structure
A_2BO_4	K_2NiF_4-typed structure
TEC	Thermal expansion coefficients
$p(O_2)$	Partial pressure of oxygen
8-YSZ	8 mol% Y_2O_3-stabilized ZrO_2
TPB	Three-phases boundary
SDC	Samaria-doped ceria
GDC	Gadolinia-doped ceria
LSM	Perovskite containing La,Sr, and Mn
LNF	Perovskite containing La,Ni, and Fe
LSC	Perovskite containing La,Sr, and Co
LSCA	Perovskite and K_2NiF_4-typed oxides containing La,Sr,Co, and Al
LSA	Perovskite containing La,Sr, and Al

LIST OF SCHEMES

CHAPTER I
INTRODUCTION

1.1   Background

Nowadays, the electricity is commonly generated by burning natural fuel such as petroleum and coal, nuclear generator, hydroelectric conventional and renewable. The energy demand keeps going up due to the increase of human population and the rapid development of technology. Figure 1.1 shows world primary energy demand and its extrapolation to the year 2030 [1] by y axis is amount of energy compared with million tons of oil equivalent, x axis is year and blue line is organization for economic co-operation and development (OECD) which is developed country. Orange area is China and India which have the most population and great power. The problem results from the natural energy sources are limited and their prices are uncontrollable and influenced by manufacturing countries and world politics.
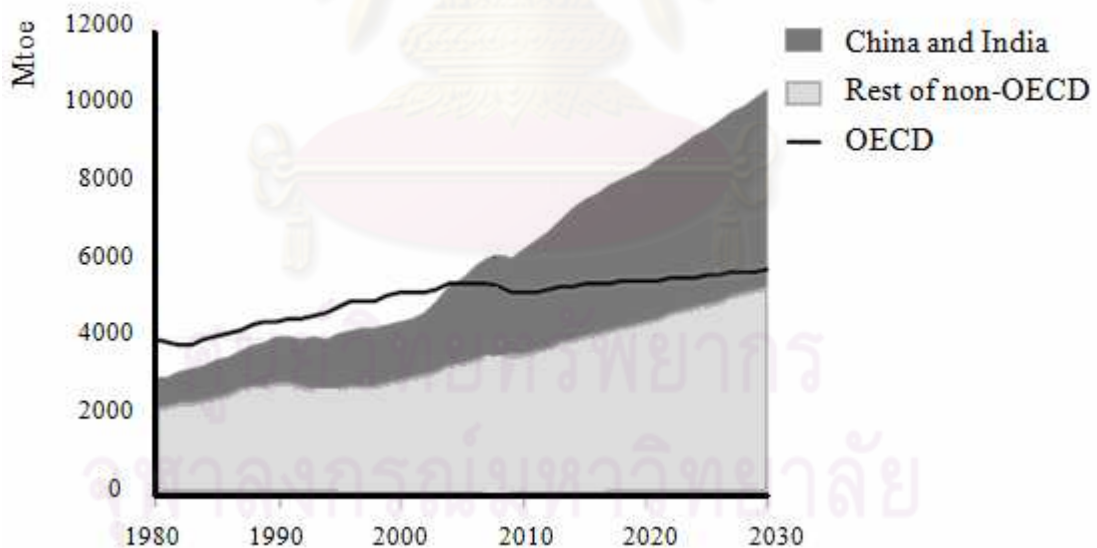
Figure 1.1   World primary energy demand [1].

Furthermore, a growing number of energy uses causes environmental impacts, such as acid rain, air pollution and global warming. Increasing amount of CO_2 caused by fossil fuel combustion is one reason for the global warming phenomenon. Figure

1.2 shows global CO_2 cycle. The number in figure is amount of carbon in carbon compound term in billion of tons. Amount of carbon flux form anthropogenic flux turn to atmosphere have higher than return to ground as a result carbon compound in carbon dioxide or carbon monoxide accumulate as green house gas cause global worming effect. Therefore, alternative energy sources those are friendly for environment, such as biomass, solar cell, wind power and fuel cell, are in serious consideration.
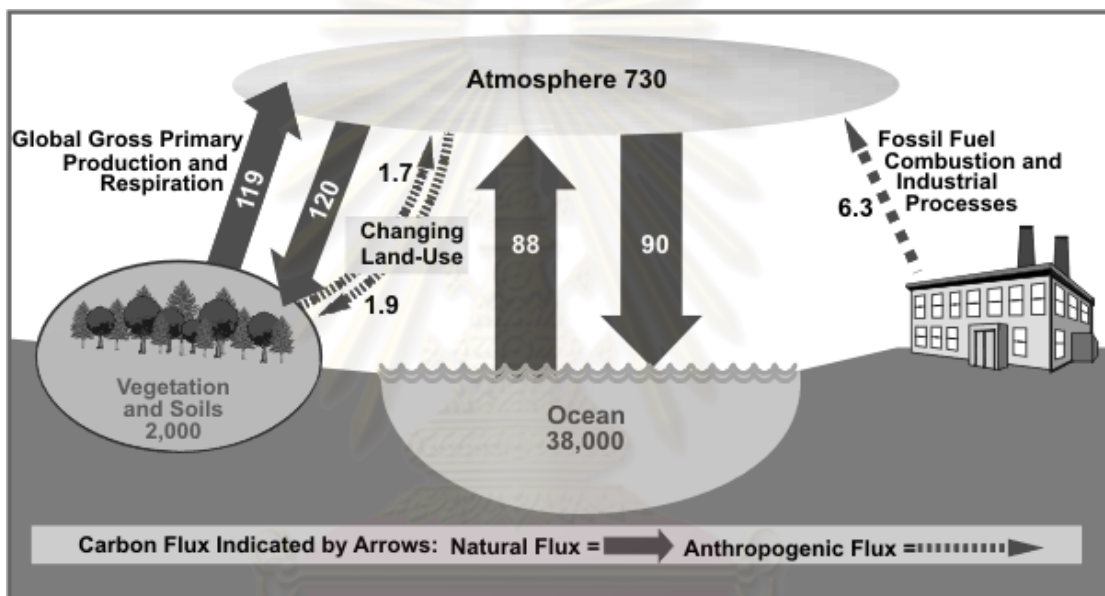
Figure 1.2 Global Carbon cycles [2].

In this thesis, fuel cell is of interest. A fuel cell is an electrochemical device that converts the chemical energy in fuels to electricity. By-products of fuel cell are pure water and heat that also could be used in other applications. The impact on environmental issue makes fuel cell become the great interest of green energy sources. Types of fuel cell are classified by an operating temperature, a type of electrolyte, a type of fuel, a type of chemical reaction and type of catalyst required.

Solid oxide fuel cells (SOFCs) contain a ceramic electrolyte and operate at high temperature about 800 – 1000°C. SOFCs are considered as a promising device to convert energy with high efficiency about 45 – 65 %. Moreover, various fuels, such as alcohol, methane, hydrogen, could be used without purification. The most common materials used for SOFC are an oxide ion conducting yttria-stabilized zirconia (YSZ)

as an electrolyte, strontium-doped lanthanum magnanite (LSM) as a cathode, nickel/YSZ as an anode, and doped lanthanum chromite or refractory metals as interconnect materials. Operating at high temperature presents some problems such as thermal stability and chemical stability of electrode materials Therefore, it is important to develop the electrode materials with higher thermal stability and chemical stability. The aim of this thesis is to search for new cathode candidates by investigating the changes of structures and morphology related to the chemical stability with the electrolyte at operating temperatures. The desired properties of cathode materials include high-electronic and ionic conductivities, adequate porosity for gas transport, high thermal stability and chemical compatibilities with the electrolyte, and long-term stability. With these requirements, the mixed ionic–electronic conductors such as perovskite (ABO_3) and K_2NiF_4-typed structure (A_2BO_4) [3] have been widely investigated for their potential application as cathode materials [4].

1.2 Literature reviews of cathode materials

1.2.1 Literature reviews of perovskite-typed oxides

One of the main SOFC components is a cathode. In particular, perovskite materials are well known for their more than adequate characteristics as solid oxide fuel cell (SOFC) cathode materials. Sr-doped $LaMnO_3$ (LSM) has been widely studied as a cathode material, primarily due to its relatively high electrocatalytic activity for O_2 reduction and good thermal stability but less chemical compatibility with Y_2O_3-stabilized ZrO_2 (YSZ) electrolyte [5]. Chemical reactivity between LSM and YSZ leads to the formation of the pyrochlore, $La_2Zr_2O_7$ (LZO) that reduces cathode performance because it has significantly lower conductivity than LSM or YSZ at SOFC operating temperatures [6]. An additional problem of LSM is its higher thermal expansion coefficient than YSZ, which could be solved by substituting some of the Mn ions by another cation. $La_{1-x}Sr_xMO_3$ (M = Co, Cr and Fe) were reported by Yamamoto et al [7] on the electrical conductivity and chemical compatibility with YSZ. Among these materials, $La_{1-x}Sr_xCoO_3$ (LSC) showed highest electrical conductivity but the problem was their high thermal expansion coefficient. Teraoka et al. [8] studied chemical compatibility of LSC when $Ce_{0.8}Sm_{0.2}O_{1.9}$ (SDC)

was used as an interlayer to prevent the direct contact of cathode and electrolyte; therefore, that the result showed good chemical compatibility. Kostogloudis *et al*. [9] reported the chemical compatibility of $La_{1-x}Sr_xCo_{0.2}Mn_{0.8}O_{3-\delta}$ and YSZ by mixing the two components in 1:1 mole ratio and firing at 1100°C that the result showed good chemical compatibility when the content of strontium was up to x = 0.03. These literatures indicated that LSC was a good candidate for cathode materials; however, the problems still are high thermal expansion and the need of using expensive SDC as an interlayer.

Several groups have reported the effect of Al doping on thermal expansion coefficient. Hrovat *et al*. [10] reported that substitution of Al into $LaCoO_3$, resulting in the decrease of thermal expansion coefficient of the perovskites with increasing content Al from 21.6×10^{-6}/K to 10.7×10^{-6}/K. Similarly, Marozau *et al*. [12] investigated effect of doping Al on $Sr_{0.7}Ce_{0.3}Mn_{1-x}Al_xO_3$. It was found that increasing Al content up to x = 0.2 would decrease thermal expansion coefficient from 11.8×10^{-6}/K to 10.8×10^{-6}/K. Moreover, Kajitani *et al*. [11] investigated the effect of Al doping on the electrical conductivity of $LaGa_{0.9}Mg_{0.1}O_{2.95}$ ($LaGa_{0.9-x}Al_xMg_{0.1}O_{2.95}$). This group found that the symmetry of crystal increased as the amount of Al increased, resulting in the increase of the electrical conductivity.

Perovskite and K_2NiF_4-typed structures were prepared by several methods such as Solid state reaction [14], Sol-gel [15], Citrate, Modified citrate [16] etc. In 2007, Liu *et al*. [16] investigated the synthesis method for $La_{0.6}Sr_{0.4}Co_{0.2}Fe_{0.8}O_3$ via citrate, modified citrate and solid state reaction. $La_{0.6}Sr_{0.4}Co_{0.2}Fe_{0.8}O_3$ was prepared by modified citrate and resulted in the smallest particle. Iamsa-ard [13] reported that modified nitric citrate method gave the smallest particle size (~0.17 μm) of $LaNi_{1-x}Fe_xO_3$, compared with water citrate (~0.45 μm), modified water citrate (~0.26 μm) and nitric citrate (~0.35 μm) methods.

1.2.2 Literature reviews of K_2NiF_4–typed oxides

Several groups have studied the preparation of lanthanum strontium cobalt oxide. Vashook *et al*. [17] investigated the effect of substituting La ions by Sr ions on La_2CoO_4 to improve its electrical property. The materials was synthesized via solid state method and calcined at 1000ºC. All single-phased K_2NiF_4-typed oxides were observed when x = 0.5 up to 1.50. The maximum conductivity is 160 S.cm^{-1} when x = 1. Matsuura *et al*. [18] reported the electronic conductivity of LSC series and found that $La_{0.5}Sr_{1.5}CoO_4$ showed good electronic conductivity about 500 S.cm^{-1} (E = 0.11 eV) at 700ºC. James *et al*. [19] synthesized $La_{2-x}Sr_xCoO_4$ via citric acid-ethylene glycol sol-gel method and calcined at 1100ºC. All single-phased K_2NiF_4 structure was achieved when x = 0.75 up to 1.50.

The preparation of lanthanum strontium aluminium oxide with K_2NiF_4–typed structure has not been studied. Raj *et al*. [20] synthesized $La_{2-x}Sr_xAlO_4$ via sol-gel method and calcined at 1300ºC. Single phase was observed when x = 1.0. It only had not stable crystal structure but also possessed good compatibility with an electrolyte at high temperature.

1.2.3 Literature reviews of chemical and physical compatibility of cathode with electrolyte

One of the problems that make perovskite and K_2NiF_4-typed materials suffered for being cathode materials in SOFC is their chemical compatibility with 8 mol% Y_2O_3-stabilized ZrO_2 (8-YSZ) electrolyte [21, 22]. Wandekar *et al*. [23] reported the synthesis of $La_{0.76}Sr_{0.19}Mn_{1-x}Co_xO_{3-d}$, LSMC$_x$ (x = 0.0 – 1.0) via a conventional ceramic route and their chemical compatibility with $Ce_{0.9}Gd_{0.1}O_{1.95}$ (GDC) electrolyte. It was found that, all LSMC$_x$ in this series were single-phased rhombohedral. As the amount of Co content increased, the electrical conductivity decreased and thermal expansion coefficient (TEC) increased. LSMCo$_x$ exhibited good compatibility with GDC when samarium doped CeO_2 (SDC) was used as a interlayer. Kamata *et al*. [24] investigated the compatibility between $La_{0.7}Ca_{0.3}Cr_{1-y}Co_yO_3$ (y = 0.05, 0.1 and 0.2) with YSZ and found good compatibility up to 1000ºC. Amesti *et al*. [25] observed the reactivity of Sr-doped $LaFeO_3$ (Sr-LSF) and YSZ, with SDC interlayer by X-ray diffraction technique. It was found that LSF had

good compatibility with YSZ up to 825°C; however, a new phase was formed as Sr doping content increased. The use of SDC as interlayer could help to prevent the formation of the new phase up to 1150°C. Tarancon *et al*. [26] reported chemical compatibility between $GdBaCo_2O_{5+x}$ with various electrolytes (e.g. YSZ, GDC and LSGM) by XRD. The XRD patterns showed that $GdBaCo_2O_{5+x}$ had good compatibility up to 700°C with YSZ, and 1000°C with GDC and LSGM.

From literatures mentioned above, the lanthanum strontium cobalt oxides (LSCA) for both perovskite and K_2NiF_4-typed structures have good mixed ionic and electronic conductors (MIECs) and the effect of doping Al ions could reduce thermal expansion coefficient in some materials. However, the partial substituting Co ions by Al ions on $La_{1-x}Sr_xCoO_3$ and $La_{1-x}Sr_xCoO_4$ have not been reported.

In this thesis, the lanthanum strontium cobalt aluminium oxide for both perovskites and K_2NiF_4-typed structures were investigated and the selected oxides of both structures were tested on their thermal stabilities and compatibility with 8-YSZ.

1.3 The objectives of this study

1. To prepare the single-phased $La_{1-x}Sr_xCo_{1-y}Al_yO_3$ (perovskite structure) and $La_{2-x}Sr_xCo_{1-y}Al_yO_4$ (K_2NiF_4-typed structure) with $0.0 < x, y < 1.0$ and $0.0 < x < 2.0$, $0.0 \leq y \leq 1.0$, respectively, by using the modified citrate method.

2. To study the effect of Al doping content on chemical compatibility of the $La_{1-x}Sr_xCo_{1-y}Al_yO_3$/ $La_{2-x}Sr_xCo_{1-y}Al_yO_4$ and 8-YSZ and on their thermal expansion coefficients.

CHAPTER II
THEORY

2.1　Fuel cell

Fuel cells are electrochemical devices that convert the chemical energy of fuels directly into electrical energy. Without combustion process involved, the by-products of fuel cells are only water and heat. The basic structure of fuel cells consists of dense electrolyte, porous anode, porous cathode and interconnects. The simple configuration is shown in figure 2.1. Table 2.1 shows many types of fuel cells and their characters. The type of fuel cell is classified by operating temperature, type of electrolyte, type of fuel, type of chemical reaction and type of catalyst required [27].
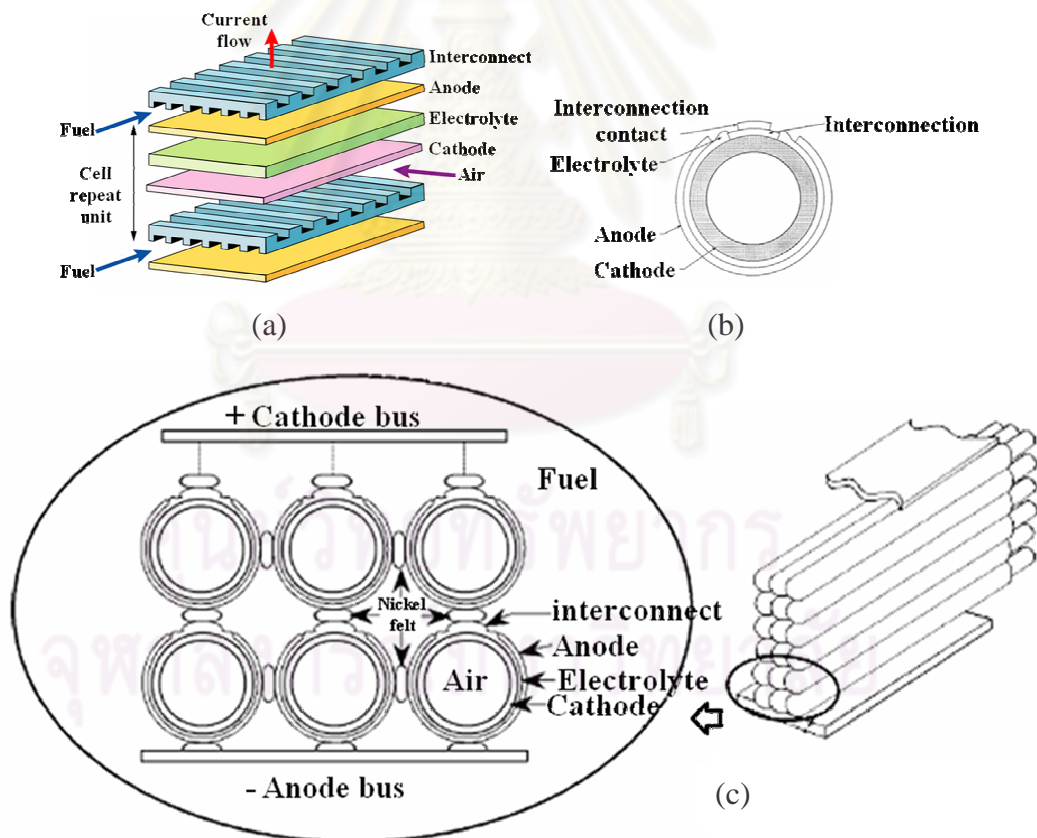
Figure 2.1　(a) flat plate of SOFC [22]

(b) Cross section of tubular configuration for SOFC [27]

(c) Cell to cell connection among tubular SOFC [27].

Table 2.1 Summaries on the different characters in various types of fuel cells [27]

	PEFC	AFC	PAFC	MCFC	ITSOFC	SOFC
Electrolyte	Ion exchange membranes	Mobilized / immobilized potassium hydroxide	Mobilized liquid phosphoric acid	Mobilized liquid molten carbonate	Ceramic	Ceramic
Operating temperature	80°C	65-220°C	205°C	650°C	600-800°C	800-1000°C
Charge carrier	H^+	OH^-	H^+	CO_3^{2-}	O^{2-}	O^{2-}
External reformer for CH$_4$	Yes	Yes	Yes	No	No	No
Catalyst	Platinum	Platinum	Platinum	Nickel	Perovskite	Perovskite

This thesis has focused on solid oxide fuel cells (SOFC). The main benefits of SOFC is its ability to comsume a wide variety of fuels directly, without purification, and gives high efficiency about 45 – 65 % that is higher than other kinds of fuel cells and other alternative energy sources as shown in table 2.2.

Table 2.2 Distribution of electric power systems [27]

Type	Qualified power	Efficiency, %
Reciprocating engines	50 kW – 6MW	33 – 37
Micro turbines	10 kW – 300 kW	20 – 30
PAFC	50 kW – 1 MW	40
SOFC	5 kW – 3 MW	45 – 65
PEM	<1 kW – 1MW	34 – 36
Photovoltaic (PV)	1 kW – 1 MW	NA
Wind turbines	150 kW – 500 kW	NA
Hybrid renewable	<1 kW – 1MW	40 – 50
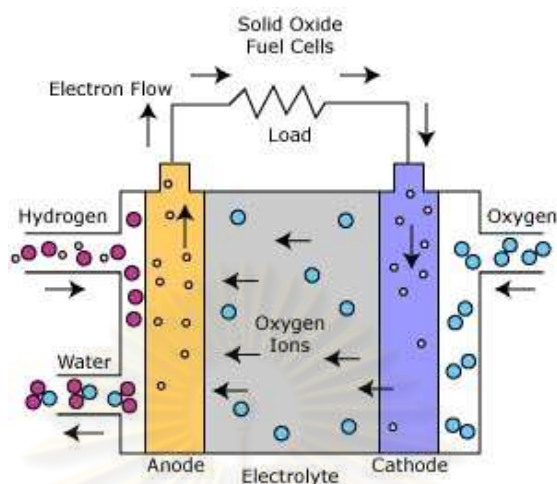
Figure 2.2 Schematic of the working processes in solid oxide fuel cell [28].

A schematic representation of SOFC with the reactant/product gases and the ion conduction flow directions though the cell is shown in figure 2.2. The mechanism of SOFC could start with that the continuous feeding of an oxidant (normally oxygen from air) to the cathode where the reduction of an oxidant to oxide ions occurred at the surface of porous cathode. Then, the oxide ions diffuse though a dense oxide-conducting electrolyte to encounter with gaseous fuels at the interface of an anode and an electrolyte. The fuel that is continuously fed at anode is oxidized by the oxide ions from an electrolyte and produces water, heat and electrons. Of the produced electrons flows from anode to cathode via an external electric circuit, and then react with an oxidant at the cathode. In this process cycle, the oxidants and fuels are consumed. The electrochemical reactions are described as followings;

$$\text{At an anode:} \quad 2H_2 + 2O^{2-} \rightarrow 2H_2O + 4e^- \quad (2.1)$$
$$\text{At a cathode:} \quad O_2 + 4e^- \rightarrow 2O^{2-} \quad (2.2)$$
$$\text{Overall reaction:} \quad 2H_2 + O_2 \rightarrow 2H_2O \quad (2.3)$$
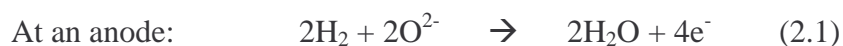
2.2 SOFC components

2.2.1 Cathode and anode

In SOFC, the operation at high temperature requires the candidate electrode materials having the following properties [29].

i. Catalytic activity. The electrode should catalyze the electrochemical and chemical reactions. Those are, for cathode, oxygen adsorption, dissociation reactions. And for anode, electrochemical oxidation of H_2 or hydrocarbon must be catalyzed.

ii. Mixed ionic and electronic conductivity.

iii. Chemical stability and compatibility with an electrolyte. The material should maintain its original properties in contact with an electrolyte at operating temperatures.

iv. High morphological stability. Normally, the high operating temperatures lead to a decrease in the active reaction sites of electrode materials.

v. Mechanical compatibility with an electrolyte. Thermal expansion mismatch between SOFC components may cause the breakdown of the cell.

vi. Low cost.

2.2.2 Electrolyte

Operating at high temperature has many advantages such as high power efficiency and various choices of fuel. The electrolyte material for SOFC is ion-conducting ceramics. The requirements for electrolyte materials are listed below [29].

i. High oxide ion conductivity.

ii. Low electronic conductivity. In order to prevent a short circuit, electrolyte must be low electronic conductive. The electronic conductivity would cause voltage loss and oxygen leakage.

iii. Chemical stability. Not only thermodynamic stability in air and fuel, but the stability under the oxygen potential gradient is also required.

iv. Mechanical strength. Mechanical strength of an electrolyte depends on the cell design and heating/cooling rates. The electrolyte materials should withstand those stresses.

v. Low cost.

Yttria - stabilized zirconia (YSZ) has been the most popular electrolyte in SOFC. Although other oxide ion conductors, such as CeO_2 or $LaGaO_3$ based oxides, show higher ionic conductivities than zirconia but they could withstand the operation at lower temperatures [29, 30].

2.3   Cathode materials

Various noble metals and oxides have been investigated as candidates for cathode materials. Platinum is one of the most popular standard electrodes for both cathode and anode; however, it has high cost. Gold and silver are alternate materials but both of them are less active than platinum and also melt at operating temperatures about 961°C [29]. Among various oxides, perovskite and K_2NiF_4-typed oxides have high potential because both of them show good catalytic activities for oxygen reduction and possess mixed ionic – electronic conductivity (MIEC).

2.3.1   Perovskite structure

Perovskites are metal oxides having a simple formula of ABO_3, A = bigger cations (e.g. La^{+3}, Sr^{+3} alkali, alkaline earth) and B = smaller cations (e.g. Mn^{+2}, Co^{+2}, Fe^{+2}, transition metal). Figure 2.3 shows the simple drawing of perovskite structure. A cations at A – site is surrounded by eight cations of B - site and twelve oxide ions. Perovskite structure could be described that the ions at A – sites and oxide ions are packed as cubic close packing (*ccp*) with ions at B – sites occupying the octahedral holes.
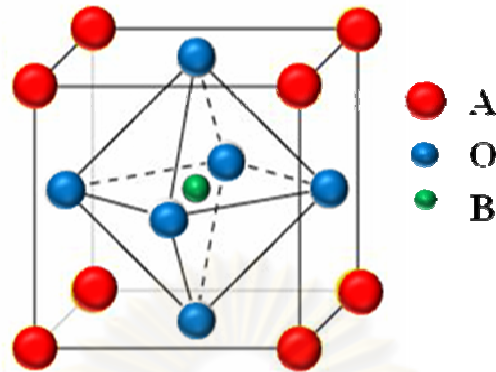
Figure 2.3 Simple drawing of perovskite structure (ABO_3).

The ideal perovskite has a cubic structure. Materials with perovskite structure could be predicted by the tolerance factor (t). The tolerance factor is related to the relationship between ionic radii of cationic constitutions. Figure 2.4 shows the relationship between ionic radii in the perovskite, which lead to the equation 2.7 in order to calculate the tolerance factor. The t values should equal to 1 for an ideal perovskitel however, from the observation t values of perovskites are normally in the range of 0.8-0.9. Once of factor as important as tolerance factor for predict cubic perovskite is octahedral factor. As seen in figure 2.4, the B-site cation fills in the octahedral hole. In a cubic, the radii of oxide ion is about 1.4 Å; therefore, the ratio of the ionic radii r_B/r_O should be varied with the limited range of 0.414 – 0.732 [31, 32].

$$a = \frac{1}{\sqrt{2}} \times 2\,(A-O) = \sqrt{2}\,(r_A + r_O) \tag{2.4}$$

$$a = 2 \times (B - O) = 2(r_B + r_O) \tag{2.5}$$

$$2(r_B + r_O) = \sqrt{2}\,(r_A + r_O) \tag{2.6}$$

Hence, $\qquad t = \dfrac{(r_A + r_O)}{\sqrt{2}(r_B + r_O)} \tag{2.7}$
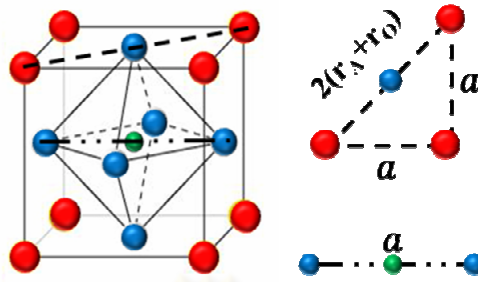
Figure 2.4 Relationship between ionic radii in the perovskite relating to the tolerance factor.

2.3.2 K$_2$NiF$_4$–typed structure

Various oxide compounds could possess K$_2$NiF$_4$-typed structure. Firstly found for K$_2$NiF$_4$ compound, the common formula of the oxide series could be written as A$_2$BO$_4$. The structure can be described as the alternate stacking of perovskite layer and rock salt (AO) layer as shown in figure 2.5.
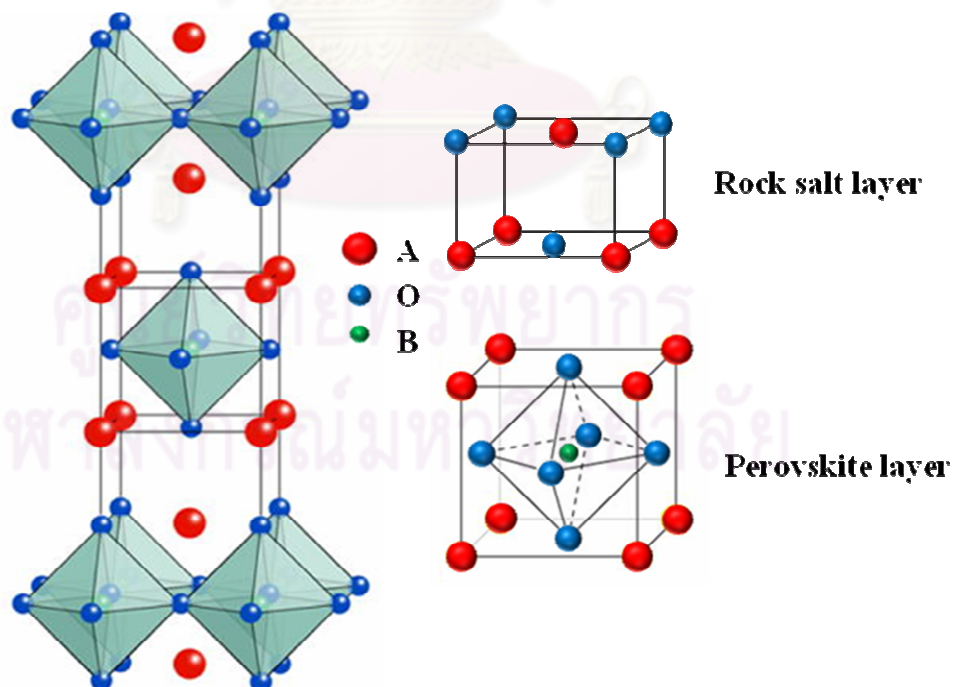
Figure 2.5 Simple drawing of K$_2$NiF$_4$ – typed structure.

Chin *et al* [33] investigated the effect of tolerance factor towards K_2NiF_4-typed oxides and reported that the *t* value rule could be applied for K_2NiF_4-typed structure with t criteria range of 0.87 – 0.99. The group represent new model to calculate more suitable tolerance factor (*tf*) using an equation 2.8. When r_O, r_A and r_B is radius of ions at O – site A – site, and B – site, respectively. The K_2NiF_4-typed structure is possible when *tf* is more than 1.00.

$$tf = \frac{\left[(3\sqrt{2} + 2\sqrt{6})r_O + 2\sqrt{6}r_A\right]}{9(r_B + r_O)}$$

(2.8)

2.4 Powder synthesis

There are many routes to synthesis powder perovskite and K_2NiF_4-typed oxides. Commonly used methods are divided into conventional solid-state reaction, co-precipitation, sol-gel synthesis, solvothermal synthesis, and combustion synthesis [34].

Solid state reaction

This method is oldest, simplest and most widely used. The preparation by mixed together of powder reactant then heat in the furnace for long periods. Advantage of this method is uncomplicated step of preparation of reactant but for the desired product must be use high temperature and long time period due to they are very inhomogeneous on the atomic level [34].

Co-precipitation

Co-precipitation is the method which separated ion or molecule from solution. The ion or molecule are precipitated by slowly add precipitant or change temperature or pressure which decrease the solubility of ion or molecule. Advantage of this method is the nanoparticle product. However the solubilities of reactants in the solution have to proportional [35].

Sol-gel synthesis

Starting point is to prepare a homogeneous solution containing all the cationic ingredients. The solution is gradually dried and transform to viscous sol containing particles of colloidal dimensions and finally amorphous solid, know as a gel, were

received then gel is fired at high temperatures to remove various volatile components and crystallize is the final product. Advantage of this method is homogeneous of cationic reactant on atomic level but reactant must be metal organic compounds which are dissolved by water [34].

Solvothermal synthesis

Solvothermal or hydrothermal synthesis is the method which involves heating the reactants in water/steam at high pressures and temperatures. The reactant and water are placed inside a Teflon-lined cylinder which is either sealed or connected to an external pressure control. Advantage of this method is require low temperature about 100 – 500ºC but these is complicated due to must be control pressure and trial and error appropriate condition, temperature and pressure [34].

Combustion synthesis

This method, starting materials are chosen that react together highly exothermically. There for once a reaction is initiated which enough heat is generated for a very high temperature to complete reaction occurs rapidly. Advantages of this method are using widely kind of reactant, giving small particle size of product and homogeneous solution of cationic reactants on atomic level but must be required fuel and oxidant for self combustion [34].

2.5   Thermal expansion

Thermal expansion is an important property of materials used in consideration of choosing electrodes and electrolytes for SOFC. Materials usually expand or shrink upon heating depending on lattice rigidity and structural changes. Different degrees of thermal expansion could cause the mechanical mismatch of each component and lead to the breakdown of SOFC cell.

Thermal expansion coefficient (α_1) is the term that indicates the degree of expansion in one direction. The unit of α_1 is K^{-1}or C^{-1}. The α_1 value is calculated according to figure 2.6 and equation 2.11 [36].
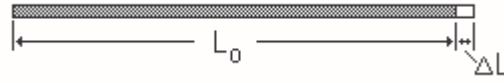
Figure 2.6 Linear expansion.

$$(L_f - L_0)/L_0 = \alpha_1 (T_f - T_0) \tag{2.9}$$

$$\Delta L/L_0 = \alpha_1 \Delta T \tag{2.10}$$

$$\alpha_1 = 1/L_0 \times (\Delta L/\Delta T) \tag{2.11}$$

Where, L_0 is an original length (mm).

L_f is a final length (mm).

T_0 is a starting temperature.

T_f is a final temperature.

2.6   Characterization of materials

X-ray diffraction (XRD) is one of the physical methods normally used for phase purity analysis and structure determination of crystalline solids [37].

The most important theory in XRD would be the Bragg equation:

$$n\lambda = 2d\sin\theta \tag{2.12},$$

where d is an interplanar spacing between the crystal planes, n is an integer, λ is the wavelength of the X-rays, and θ is the diffraction angle. λ and d are measured in the same units, usually in angstroms.

When already defined d spacing of a set of planes is determined by XRD and the type of lattice is selected, the relationships of d spacing, miller indices (*hkl*) and lattice parameters (*a*, *b*, *c*) are related in an equation according to the type of lattice. The general equation is triclinic crystal.

$$\frac{1}{d^2} = \frac{1}{V^2}(S_{11}h^2 + S_{22}k^2 + S_{33}l^2 + 2S_{12}hk + 2S_{23}kl + 2S_{13}hl) \tag{2.13}$$

Where,

$$V = abc\sqrt{1 - \cos^2\alpha - \cos^2\beta - \cos^2\gamma + 2\cos\alpha\cos\beta\cos\gamma} \tag{2.14}$$

$$S_{11} = b^2 c^2 \sin^2\alpha$$

(2.15)

$$S_{22} = a^2 c^2 \sin^2\beta$$

(2.16)

$$S_{33} = a^2 b^2 \sin^2\gamma$$

(2.17)

$$S_{12} = abc^2(\cos\alpha \cos\beta - \cos\gamma)$$

(2.18)

$$S_{23} = a^2 bc (\cos\beta \cos\gamma - \cos\alpha)$$

(2.19)

$$S_{13} = ab^2 c (\cos\gamma \cos\alpha - \cos\beta)$$

(2.20)

For an orthorhombic lattice, α, β and γ = 90°, the equation 2.14 is simplified to:

$$\frac{1}{d_{hkl}^2} = \frac{h^2}{a^2} + \frac{k^2}{b^2} + \frac{l^2}{c^2}$$

(2.21)

For a cubic lattice, $a = b = c$; hence,

$$\frac{1}{d_{hkl}^2} = \frac{h^2 + k^2 + l^2}{a^2}$$

(2.22)

CHAPTER III
EXPERIMENTAL

3.1   Chemicals:

Table 3.1 Chemicals and reagents

Reagents	Formula weight	Purity (%)	Company
$La(NO_3)_3.6H_2O$	433.03	> 99	Fluka
$Sr(NO_3)_2$	211.63	> 99	Acros organics
$Co(NO_3)_2.6H_2O$	291.03	> 98	Univar
$Al(NO_3)_3.9H_2O$	375.13	98	Unilab
Citric acid	192.13	> 99.5	Aldrich
Ammonia solution	35.00	25	Merck
HNO_3	63.01	65	Merck
8 mol %ZrO_2/Y_2O_3	123.22	99.9	Aldrich

3.2   Synthesis of perovskite and K_2NiF_4-typed powders by modified nitric citrate method

The perovskite $La_{1-x}Sr_xCo_{1-y}Al_yO_3$ (0.0 < x, y < 1.0) and the K_2NiF_4-typed $La_{2-x}Sr_xCo_{1-y}Al_yO_4$ (0.0 < x < 2.0 and 0.0 ≤ y ≤ 1.0) (LSCA) were synthesized. The stoichiometric amounts of $La(NO_3)_3.6H_2O$, $Sr(NO_3)_2$, $Co(NO_3)_2.6H_2O$ and $Al(NO_3)_3.9H_2O$ were dissolved in HNO_3 and H_2O in the volume ratio of 1:1. The citric acid was added with the citric acid to nitrate mole ratio of 2:1 for perovskite powders, and that of 1:1 for K_2NiF_4-typed powders. Aqueous NH_3 (~45 mL) was slowly added into the mixture solution at the controlled rate of 2 – 3 ml/min. The pH of the solution was adjusted to approximately 8 – 10. The mixture solution was stirred for 3 – 5 h.

The homogeneous mixture solution was placed in a two-liter beaker covered with a fine sieve to prevent the loss of fine powder during combustion. The combustion was carried out on a hot plate with the heater temperature of 200 – 300°C. Upon heating, water was evaporated until a sticky gel was obtained. Then it became a sticky mass before self-ignition. The combustion lasted for about 10 – 20 seconds. At the end, a sponge-like black solid expanded in the beaker. The products were grinded by a mortar for 10 – 15 min until a fine powder was obtained. The obtained black

powders were calcined at 900 – 1200°C with the increasing rate of 2°C/min for 5h to yield the desired $La_{1-x}Sr_xCo_{1-y}Al_yO_3$ and $La_{2-x}Sr_xCo_{1-y}Al_yO_4$ samples.

$La(NO)_3.6H_2O$	$Sr(NO_3)_2$	$Co(NO_3)_2.6H_2O$	$Al(NO_3)_3.9H_2O$

Dissolve in water and conc. HNO_3.
Add citric acid.
Slowly add aq. NH_3 until pH ∼8 – 10.

Mixed solution

Heat at 200˚C until dryness.

As-synthesized LSCA

Calcine at 900 – 1200°C for 5 h, at the heating rate of 2°C/min.

Calcined LSCA
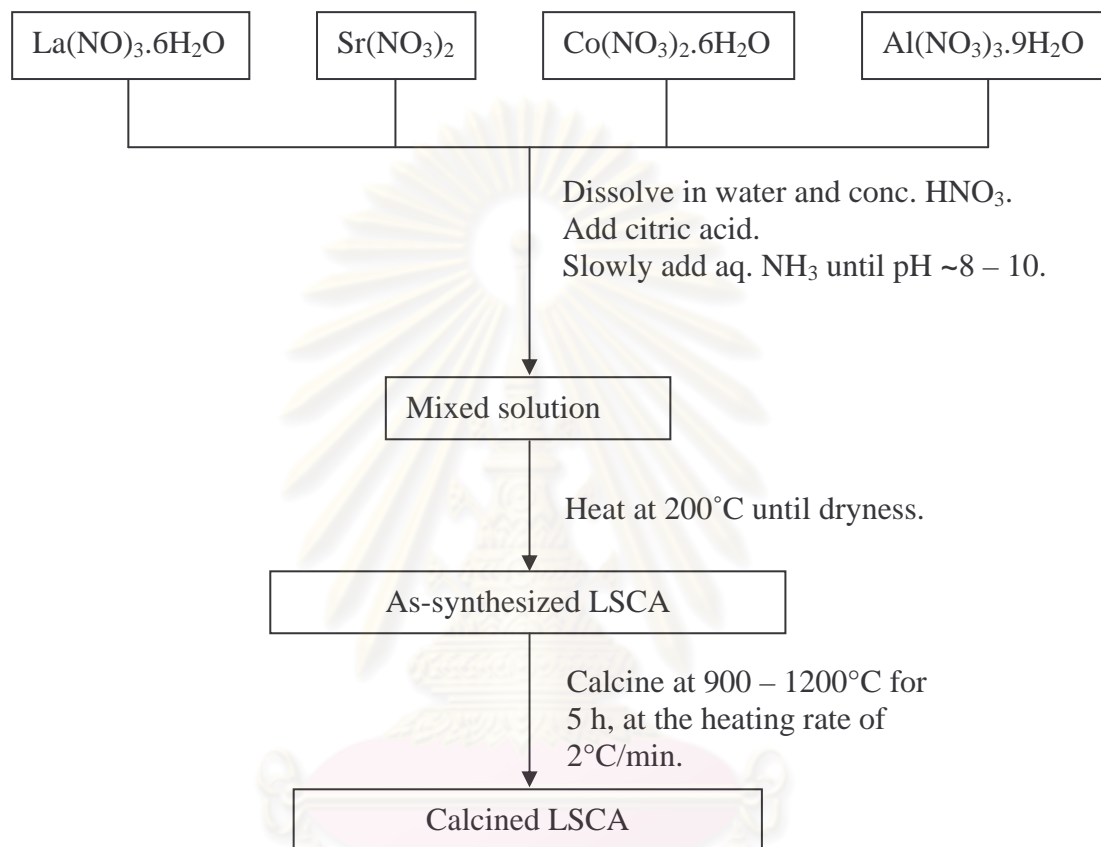
Scheme 3.1 The preparation procedure of $La_{1-x}Sr_xCo_{1-y}Al_yO_3$ and $La_{1-x}Sr_xCo_{1-y}Al_yO_4$ (LSCA).

Table 3.2 A list of the experimental conditions and results for the synthesis of perovskite compounds by modified citrate method

Materials	Color and appearance changing during adding NH_3	pH	Total combustion period (min) and material appearance	Calcination temperature (°C)
$La_{1-x}Sr_xCoO_3$	Red to violet to yellow to orange to dark brown	9.28	40 / black powder	900
$La_{1-x}Sr_xCo_{0.95}Al_{0.05}O_3$	Red to violet to yellow to orange to dark brown	9.44	45 / black powder	900
$La_{1-x}Sr_xCo_{0.9}Al_{0.1}O_3$	Red to violet to yellow to orange to dark brown	9.32	40 / black powder	900
$La_{1-x}Sr_xCo_{0.8}Al_{0.2}O_3$	Red to violet to orange to dark brown	9.27	55 / black powder	900
$La_{1-x}Sr_xCo_{0.7}Al_{0.3}O_3$	Red to violet to orange to dark brown	9.28	50 / black powder	900
$La_{1-x}Sr_xCo_{0.6}Al_{0.4}O_3$	Red to violet to orange to dark brown	9.24	55 / black powder	900
$La_{1-x}Sr_xCo_{0.5}Al_{0.5}O_3$	Red to violet to orange to dark brown	9.29	50 / black powder	900
$La_{1-x}Sr_xCo_{0.4}Al_{0.6}O_3$	Red to pink to violet to orange to dark brown	9.37	40 / black powder	900
$La_{1-x}Sr_xCo_{0.3}Al_{0.7}O_3$	Red to pink to violet to orange to dark brown	9.22	50 / black powder	900
$La_{1-x}Sr_xCo_{0.2}Al_{0.8}O_3$	Red to pink to violet to orange to brown	9.35	45 / brown powder	900
$La_{1-x}Sr_xCo_{0.1}Al_{0.9}O_3$	Red to pink to violet to orange to brown	9.38	50 / brown powder	900
$La_{1-x}Sr_xAlO_3$	Red to pink to violet to orange to brown	9.25	45 / white powder	900

Table 3.3 A list of the experimental conditions and results for the synthesis of K_2NiF_4-structure compounds by modified citrate method

Materials	Color and appearance changing during adding NH_3	pH	Total combustion period (min) and material appearance	Calcination temperature (°C)
$La_{2-x}Sr_xCoO_3$	Red to orange to dark brown	9.23	30 / black powder	900
$La_{2-x}Sr_xCo_{0.95}Al_{0.05}O_4$	Red to orange to dark brown	9.20	35 / black powder	900
$La_{2-x}Sr_xCo_{0.9}Al_{0.1}O_4$	Red to orange to dark brown	9.20	40 / black powder	900
$La_{2-x}Sr_xCo_{0.8}Al_{0.2}O_4$	Dark pink to orange to dark brown	9.29	35 / black powder	900
$La_{2-x}Sr_xCo_{0.7}Al_{0.3}O_4$	Dark pink to orange to dark brown	9.25	40 / dark brown powder	900
$La_{2-x}Sr_xCo_{0.6}Al_{0.4}O_4$	Dark pink to orange to dark brown	9.27	45 / brown powder	900
$La_{2-x}Sr_xCo_{0.5}Al_{0.5}O_4$	Pink to orange to brown	9.25	40 / brown powder	900
$La_{2-x}Sr_xCo_{0.4}Al_{0.6}O_4$	Light pink to orange to brown	9.27	35 / light brown powder	900
$La_{2-x}Sr_xCo_{0.3}Al_{0.7}O_4$	Light pink to orange to brown	9.25	30 / light brown powder	900
$La_{2-x}Sr_xCo_{0.2}Al_{0.8}O_4$	Light pink to orange to	9.25	35 / light brown powder	900
$La_{2-x}Sr_xCo_{0.1}Al_{0.9}O_4$	Light pink to orange to light brown	9.29	40 / light brown powder	900
$La_{2-x}Sr_xAlO_4$	Clear to clear	9.24	45 / white powder	900

3.3   Chemical compatibility

In general, a major problem in the use of cathode materials for SOFC is their reactivity with electrolyte materials, which leads to the formation of undesirable new phases along the cathode–electrolyte interface that can affect the electrical conductivity. For this reason, the study of possible reactions between the LSCA sample and YSZ was investigated by two approaches.

3.3.1   The mixtures of $La_{1-x}Sr_xCo_{1-y}Al_yO_3$ and $La_{2-x}Sr_xCo_{1-y}Al_yO_4$ powders with 8-YSZ

To study chemical reactivity of single phase of both of structure samples with yttria stabilized zirconia (8 mol % YSZ), compressed powder mixtures of both materials were investigated at elevated temperatures. The purpose of this mixing compaction was to provide maximum interfacial contact area between two reactants. To prepare pressed powder pellets, the LSCA samples and YSZ powder were mixed in 1:1 weight ratio and grinded for 15 min. The mixed powders were pressed into cylindrical pellets using a uniaxial press, and then fired at different temperatures (750 – 1100°C), each for 5 h. Phase impurities of fired pellets were determined by X-ray diffraction.

3.3.2   The membrane of 8-YSZ with the screen–printed $La_{1-x}Sr_xCo_{1-y}Al_yO_3$ and $La_{2-x}Sr_xCo_{1-y}Al_yO_4$ films

To study the interface of LSCA/YSZ couple, the powder of 8 mol % YSZ was pressed into cylindrical pellets using a uniaxial press and the obtained pellet was sintered at 1500°C for 2 h. Then, the dispersion of LSCA samples in polyethylene glycol (PEG) was screen-printed on the sintered YSZ pellet. The LSCA screen-printed YSZ pellets were fired at selected temperatures. The cross section of the pellets was monitored by SEM/EDS in order to characterize the microstructure and investigate the atomic-diffusion across the interface of LSCA and YSZ.

3.4   Thermal expansion coefficient

The physical compatibility between LSCA samples and 8-YSZ was investigated in term of the thermal expansion coefficient (TEC). The selected LSCA sample was made into a sample bar by the isostatic pressing of 3 g sample, and then the pellet was sintered at 1200°C for 5h in air. After that, the sintered bar with the size about $5 \times 14 \times 1.5$ mm was obtained from sawing off the pellets by the precision saw. The thermal expansion behavior was determined using dilatometer (NETZSCH DIL 402C) from the department of Materials Science, Faculty of Science, Chulalongkorn University. The thermal treatment started from room temperature up to 800°C in air with a heating rate of 10°C/min.

3.5   Density by Archimedes method

LSCA samples were grinded for 10 – 15 min and pressed to pellets (the pressing force about 2.5 tons/cm^2) and sintered at 1200°C for 5 h. Pellets were boiled in water for 5 h, then their densities were determined by the Archimedes method [38].

3.6   Characterization of materials

3.6.1   Powder X-ray diffraction (XRD)

The XRD patterns of LSCA samples were obtained by a Rigaku, Dmax 2200/Ultima$^+$ diffractometer, equipped with a monochromator and Cu Kα radiation. The tube voltage and current were set at 40 kV and 30 mA, respectively. The diffraction pattern was recorded in the 2-theta range from 20 to 70 degree. The scattering slit, divergent slit and receiving slit were fixed at 1 degree, 1degree and 0.15 mm respectively.

3.6.2   Scanning electron microscopy (SEM)

The atomic diffusion across the interface between LSCA samples and YSZ were monitored by a JSM-5800 LV scanning electron microscopy, Oxford Instrument (link ISIS series 300) at the Scientific and Technological Research Equipment center (STREC), Chulalongkorn University. EDX analysis with the line-scan and ID-point modes was used to determine the elements appeared on the cross-sectioned LSCA/YSZ pellets.

CHAPTER IV
RESULTS AND DISCUSSION

In this thesis, the new materials, $La_{1-x}Sr_xCo_{1-y}Al_yO_3$ perovskites and $La_{2-x}Sr_xCo_{1-y}Al_yO_4$ K_2NiF_4-typed oxides were synthesized by modified nitric citrate method. The substitutions of Co by Al and La by Sr were varied between $0.0 \leq y \leq 1.0$ and $0.0 < x < 1.0$ respectively for perovskite oxides, and between $0.0 \leq y \leq 1.0$ and $0.0 < x < 2.0$ respectively for K_2NiF_4-typed oxides. The obtained single-phased samples of both structures were tested for their chemical compatibility with YSZ using XRD and SEM. The effect of Al content on the thermal expansion coefficients (TEC) were investigated using a dilatometer.

4.1   Synthesis and characterization of LSCA
4.1.1   Perovskite powder
4.1.1.1 Crystal structure

The preparation of $La_{1-x}Sr_xCo_{1-y}Al_yO_3$ had two variables, x and y which are the stoichiometric contents of Sr and Al respectively. At first, the doping content of Al (y) in $La_{0.5}Sr_{0.5}Co_{1-y}Al_yO_3$, with the fixed amount of Sr (x), was varied. The calcination condition was at the temperature of 900°C for 5 h. The XRD patterns were shown in figure 4.1. Single-phased perovskites were found at the Al doping contents up to 0.05. At y = 0.10, the very small amount of unknown impurity was observed. At higher Al doping contents, the mixture of perovskite phase, K_2NiF_4-typed phase, $LaSrAl_3O_7$ and the unknown were found. The $La_{1-x}Sr_xCo_{1-y}Al_yO_3$ samples with y up to 0.20 were selected for the next step because they contained low amounts of impurities.
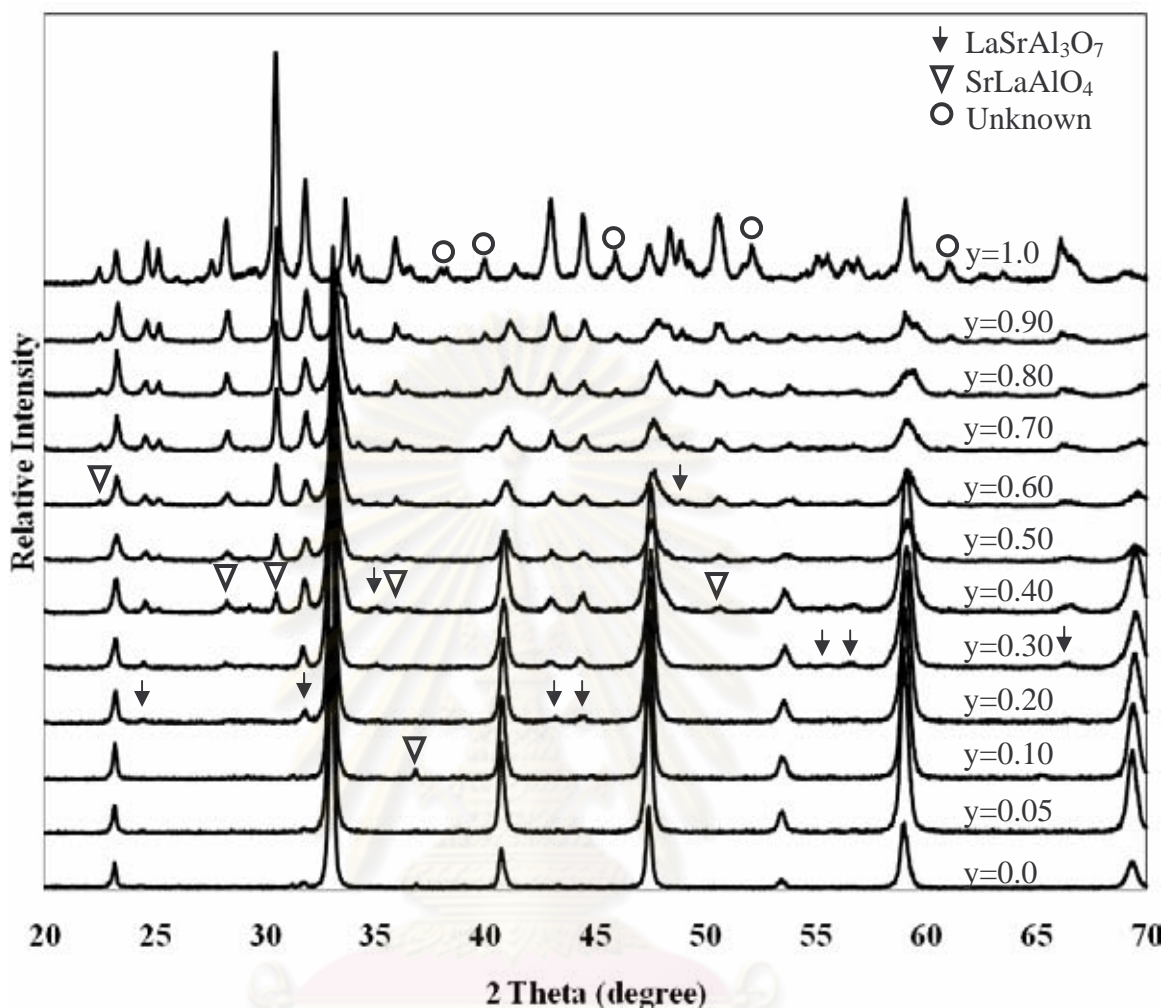
Figure 4.1 XRD patterns of $La_{0.5}Sr_{0.5}Co_{1-y}Al_yO_3$ (y = 0.0 – 1.0) calcined at 900°C for 5 h.

For the next step, the Al contents were fixed at 0.05, 0.1 and 0.2 and the Sr contents were varied from 0.0 < x < 1.0. The calcination temperature was increased to 1000°C for better diffusion efficiency of metallic elements. The XRD patterns of $La_{1-x}Sr_xCo_{0.95}Al_{0.05}O_3$, $La_{1-x}Sr_xCo_{0.9}Al_{0.1}O_3$ and $La_{1-x}Sr_xCo_{0.8}Al_{0.2}O_3$ are shown in figure. 4.2 (a), (b) and (c), respectively. The XRD patterns indicated that the desired single-phased perovskites were obtained for $La_{1-x}Sr_xCo_{0.95}Al_{0.05}O_3$ and $La_{1-x}Sr_xCo_{0.9}Al_{0.1}O_3$ at all x values ($0.1 \leq x \leq 0.9$). In the case of $La_{1-x}Sr_xCo_{0.8}Al_{0.2}O_3$, most samples, except for Sr contents of 0.5, 0.6 and 0.7, were single-phased perovskites. The impurity phases of samples with x = 0.5 – 0.7 were identified as $LaSrAl_3O_7$ (JCPDS 50-1815) and $SrLaAlO_4$ (JCPDS 24-1125). All preparation results were summarized in table 4.1.
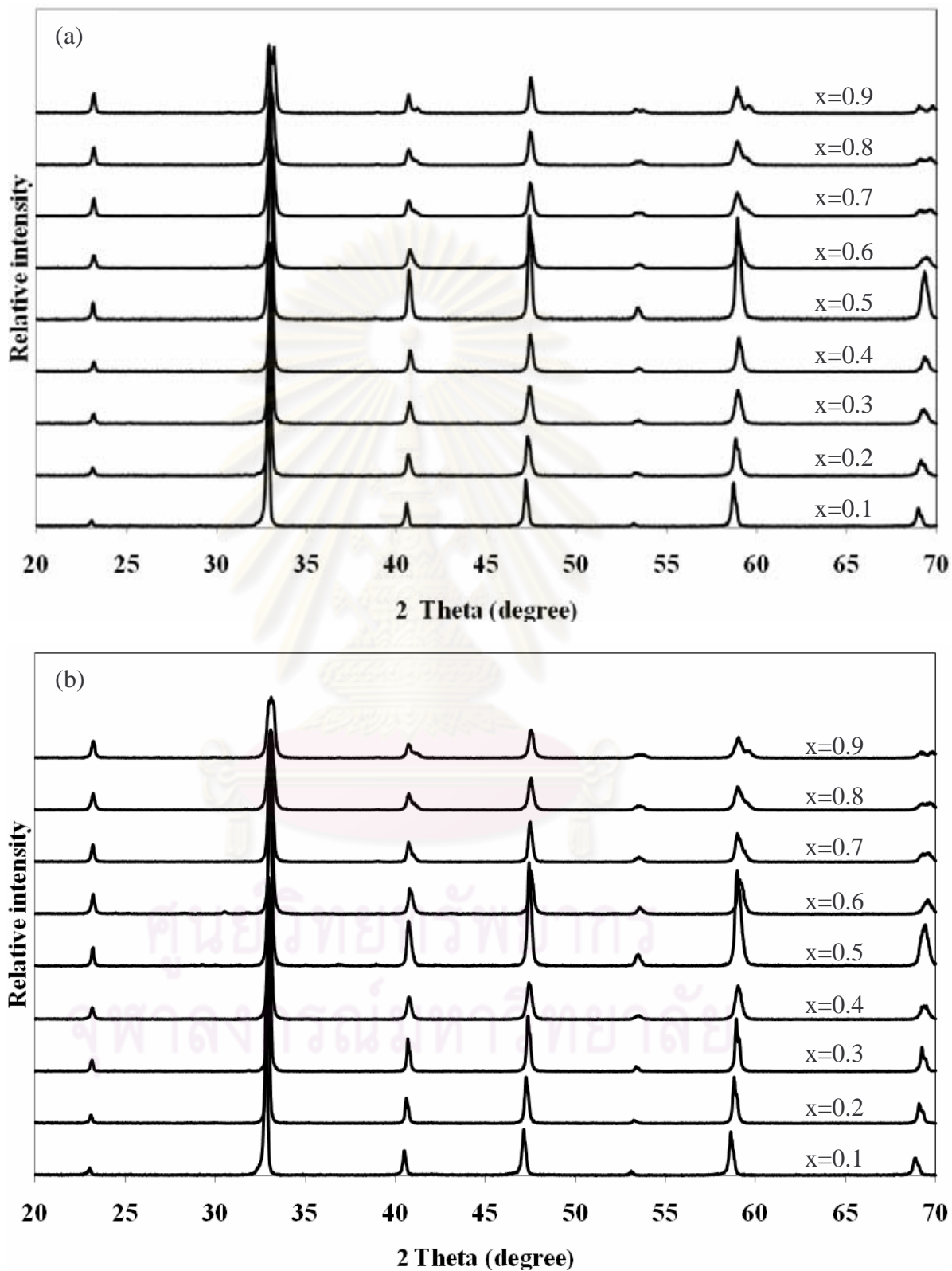
Figure 4.2 XRD patterns of (a) $La_{1-x}Sr_xCo_{0.95}Al_{0.05}O_3$, (b) $La_{1-x}Sr_xCo_{0.9}Al_{0.1}O_3$ calcined at 1000°C for 5 h.
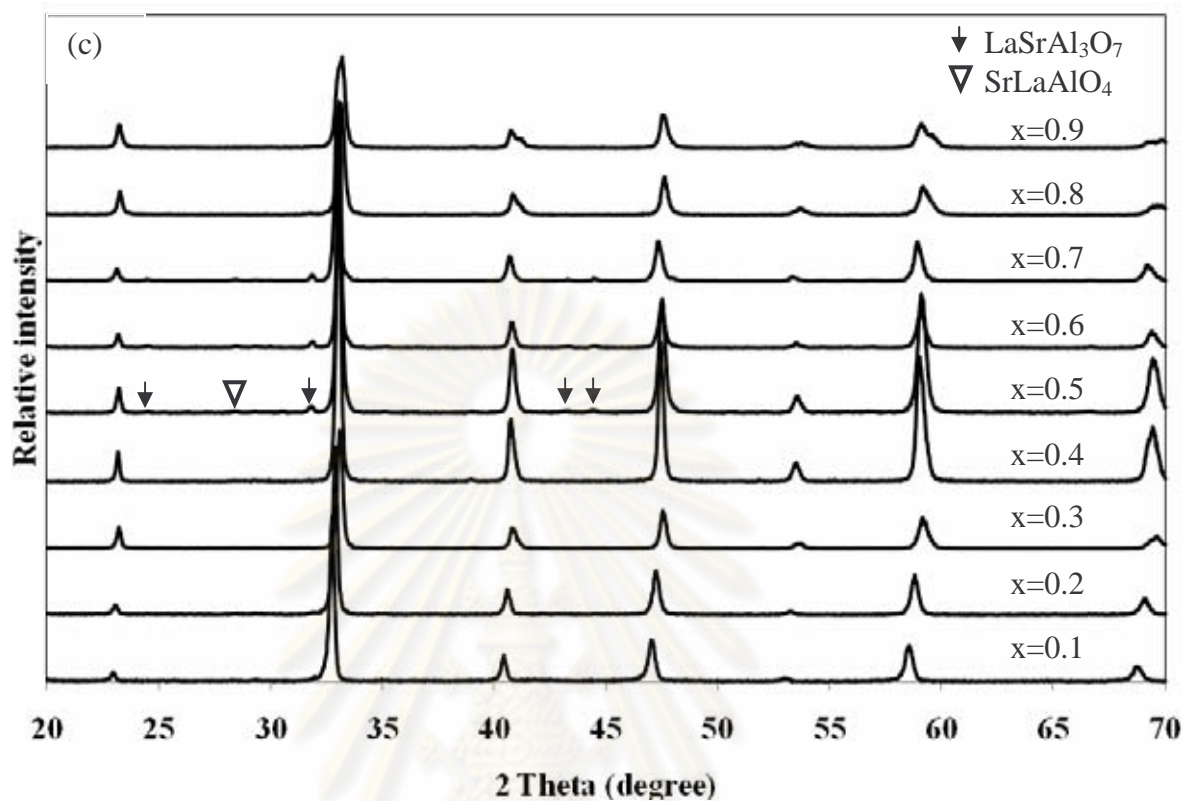
Figure 4.2 (continued) XRD patterns of (c) $La_{1-x}Sr_xCo_{0.8}Al_{0.2}O_3$ (0.0 < x < 1.0) calcined at 1000°C for 5 h.

Table 4.1 The summary of single phase perovskite samples ($La_{1-x}Sr_xCo_{1-y}Al_yO_3$)

		Al											
		1.0	0.9	0.8	0.7	0.6	0.5	0.4	0.3	0.2	0.1	0.05	0.0
	1.0									+	+	+	+
	0.9									+	+	+	+
	0.8									+	+	+	+
	0.7									+	+	+	+
Sr	0.6										+	+	+
	0.5										+	+	+
	0.4									+	+	+	+
	0.3									+	+	+	+
	0.2									+	+	+	+
	0.1									+	+	+	+
	0.0									+	+	+	+

+ is a single-phased perovskite.

The $La_{0.6}Sr_{0.4}Co_{1-y}Al_yO_3$ series were chosen in order to investigate the effect of Al doping towards lattice parameter a, unit cell volume and density because $La_{0.6}S_{0.4}CoO_3$ has been reported for its best performance as cathode materials in this series [39]. The XRD patterns of $La_{0.6}Sr_{0.4}CoO_3$, $La_{0.6}Sr_{0.4}Co_{0.95}Al_{0.05}O_3$, $La_{0.6}Sr_{0.4}Co_{0.9}Al_{0.1}O_3$ and $La_{0.6}Sr_{0.4}Co_{0.8}Al_{0.2}O_3$ are shown in figure 4.3. The patterns were indexed as the cubic perovskite structure ($a = b = c$ and $\alpha = \beta = \gamma = 90°$), and the lattice parameter was calculated from d spacings of strong peaks (*100*), (*110*), (*111*), (*200*), (*211*) and (*220*). The lattice parameters, unit cell volumes and densities were calculated from the XRD patterns were summarized in table 4.2. Figure 4.4 reveals the trends of lattice parameter and unit cell volume upon Al contents. It is clearly seen that the density of sample decreases with the increase of Al content. The density depends on the changes of two factors, a unit cell volume and a formula weight. Although the increasing in Al content results to the decrease in a unit cell due to the smaller cationic size of Al^{3+} (0.535Å) compared to Co^{3+} (0.545Å), the decrease of a formula weight as the Al contents increase dominates the decrease of unit cell values. Therefore, the overall result is the decreasing density as Al content increases. Furthermore, the relative densities of pressed samples, as the ratio of Archimedes method density and calculated density, were calculated and presented in table 4.2. The relative intensity that is greater than 90% of the theoretical value is required for the measurement of thermal expansion coefficient [40]. The results indicate that all samples have the relative densities more than 90% of the theoretical values.
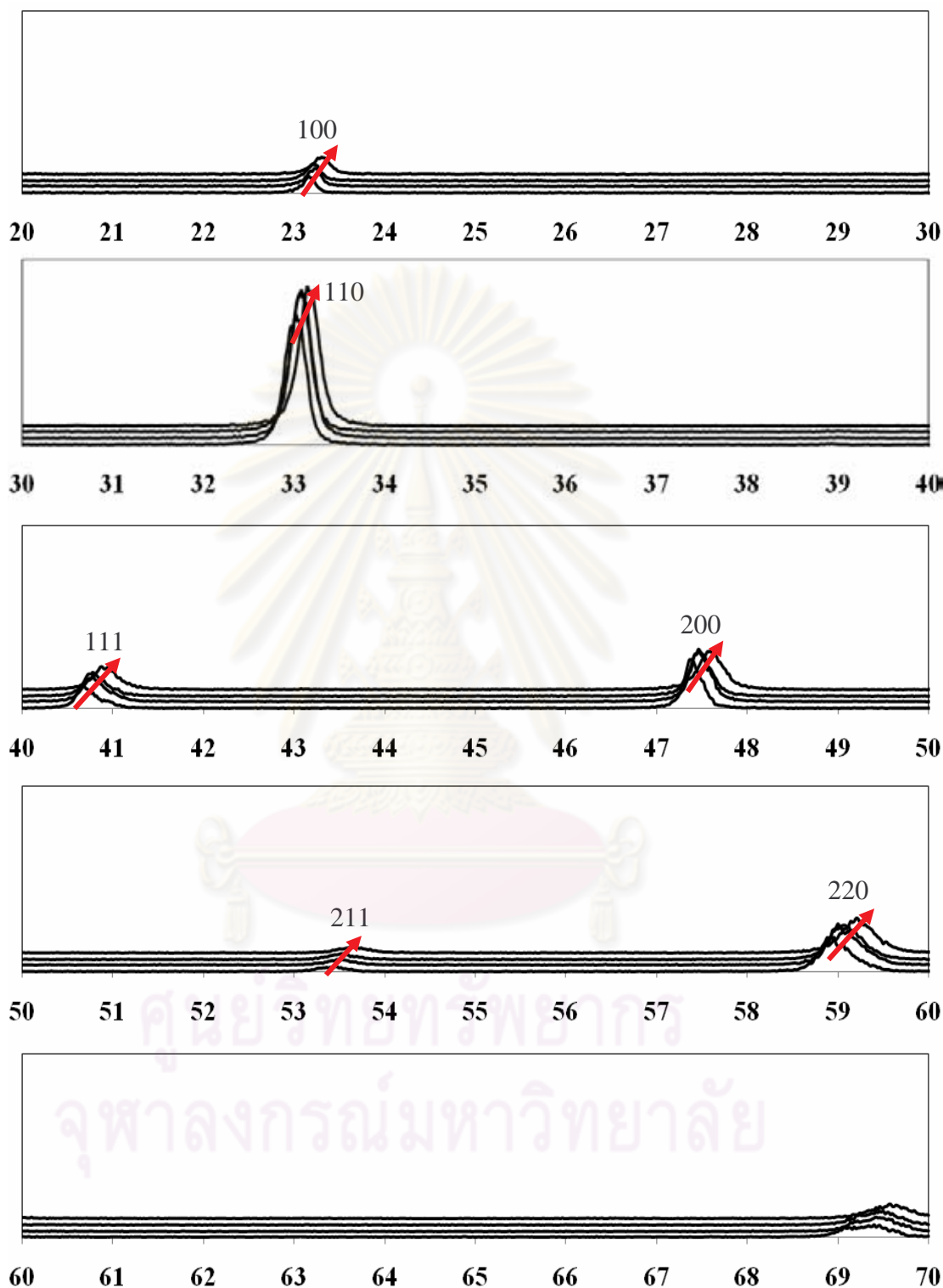
Figure 4.3 XRD patterns of perovskite series $La_{0.6}Sr_{0.4}Co_{1-y}Al_yO_3$ (y = 0.0, 0.05, 0.1 and 0.2) calcined at 1100°C for 5 h.

Table 4.2   Lattice parameters, unit cell volumes, densities, relative densities of perovskite series $La_{0.6}Sr_{0.4}Co_{1-y}Al_yO_3$ (y = 0.05, 0.1 and 0.2)

Materials	Symmetry	a (Å)	Unit cell volume (Å^3)	Density (g/cm^3)	Relative density*
$La_{0.6}Sr_{0.4}CoO_3$	Cubic	3.8348	56.4	6.1242	92.32
$La_{0.6}Sr_{0.4}Co_{0.95}Al_{0.05}O_3$	Cubic	3.8278	56.1	6.1067	92.22
$La_{0.6}Sr_{0.4}Co_{0.9}Al_{0.1}O_3$	Cubic	3.8285	56.1	6.0592	92.16
$La_{0.6}Sr_{0.4}Co_{0.8}Al_{0.2}O_3$	Cubic	3.8180	55.7	6.0020	91.96

* Relative density = (measured density/theoretical density) ×100 [41]
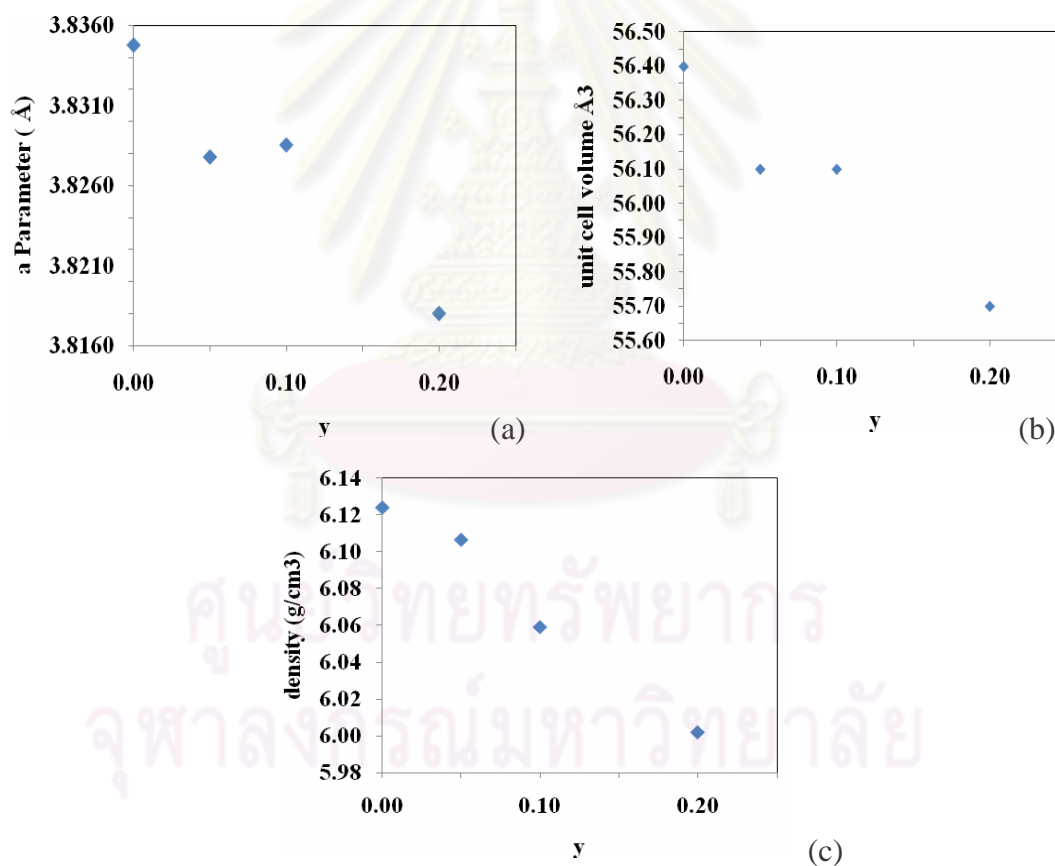
Figure 4.4   (a) Lattice parameters (b) unit cell volumes and (c) densities of perovskite series $La_{0.6}Sr_{0.4}Co_{1-y}Al_yO_3$ (y = 0.05, 0.1 and 0.2).

4.1.1.2 Morphology of perovskite

Figure 4.5 shows SEM images of perovskite particles with different Al dopant levels. The decreasing tendency of particle size with the increase of Al content is clearly seen. The particle sizes of $La_{0.6}Sr_{0.4}Co_{1-y}Al_yO_3$ (y = 0.0, 0.05, 0.1 and 0.2) are 0.65 µm, 0.50 µm, 0.36 µm and 0.28 µm respectively.
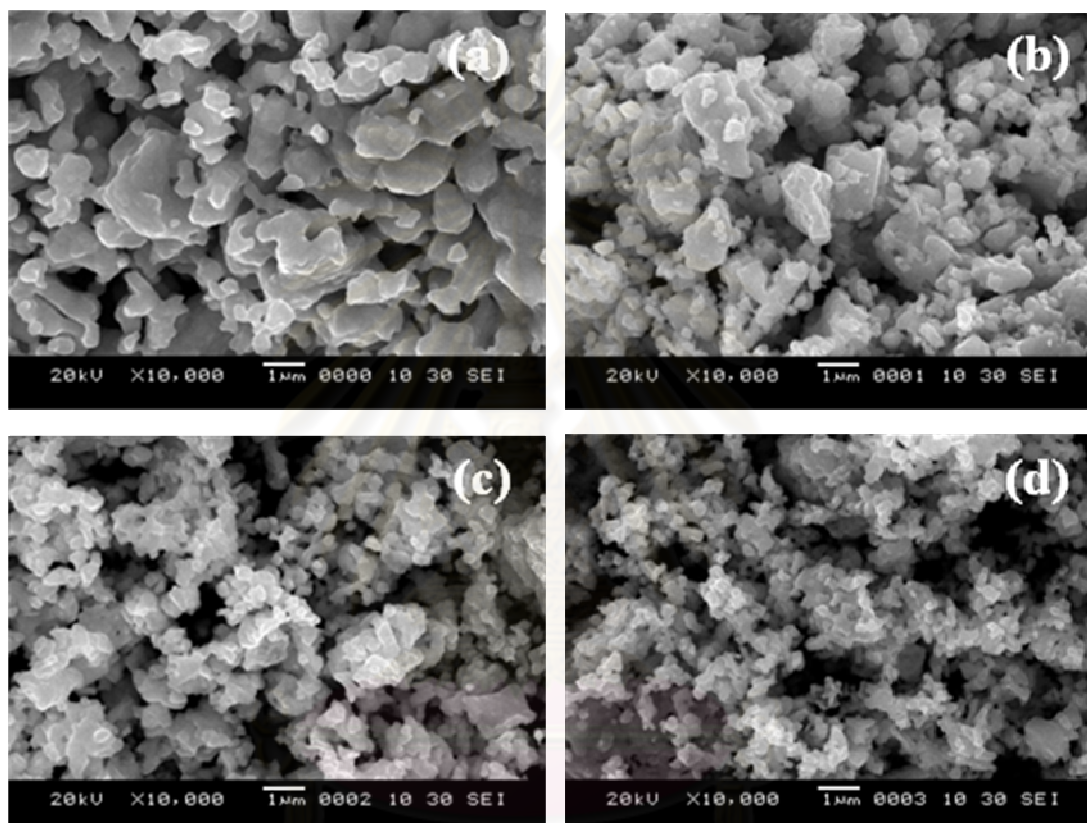
Figure 4.5 SEM images of (a) $LaSrCoO_3$, (b) $La_{0.6}Sr_{0.4}Co_{0.95}Al_{0.05}O_3$, (c) $La_{0.6}Sr_{0.4}Co_{0.9}Al_{0.1}O_3$, and (d) $La_{0.6}Sr_{0.4}Co_{0.8}Al_{0.2}O_3$ after calcination at 1000°C for 5h.

4.1.2 K₂NiF₄- typed oxide powder
4.1.2.1 Crystal structure

K_2NiF_4-typed samples were prepared in the similar procedure as perovkite samples. At first, the doping content of Al (y) in $La_{1.0}Sr_{1.0}Co_{1-y}Al_yO_4$, with the fixed amount of Sr (x = 1.0), was varied. The calcination condition was at the temperature of 900°C for 5 h. The XRD patterns were shown in figure 4.6. Single-phases were found for Al doping up to y = 0.6. At higher Al doping contents, the mixture of K_2NiF_4-typed phase, perovskite phase, $LaSrAl_3O_7$ was found. At y ≥ 0.9,

$LaAlO_3$ with the trace of La_2O_3 were found. The single-phased $La_{2-x}Sr_xCo_{0.9}Al_{0.1}O_4$ series were selected for the synthesis of various Sr contents.
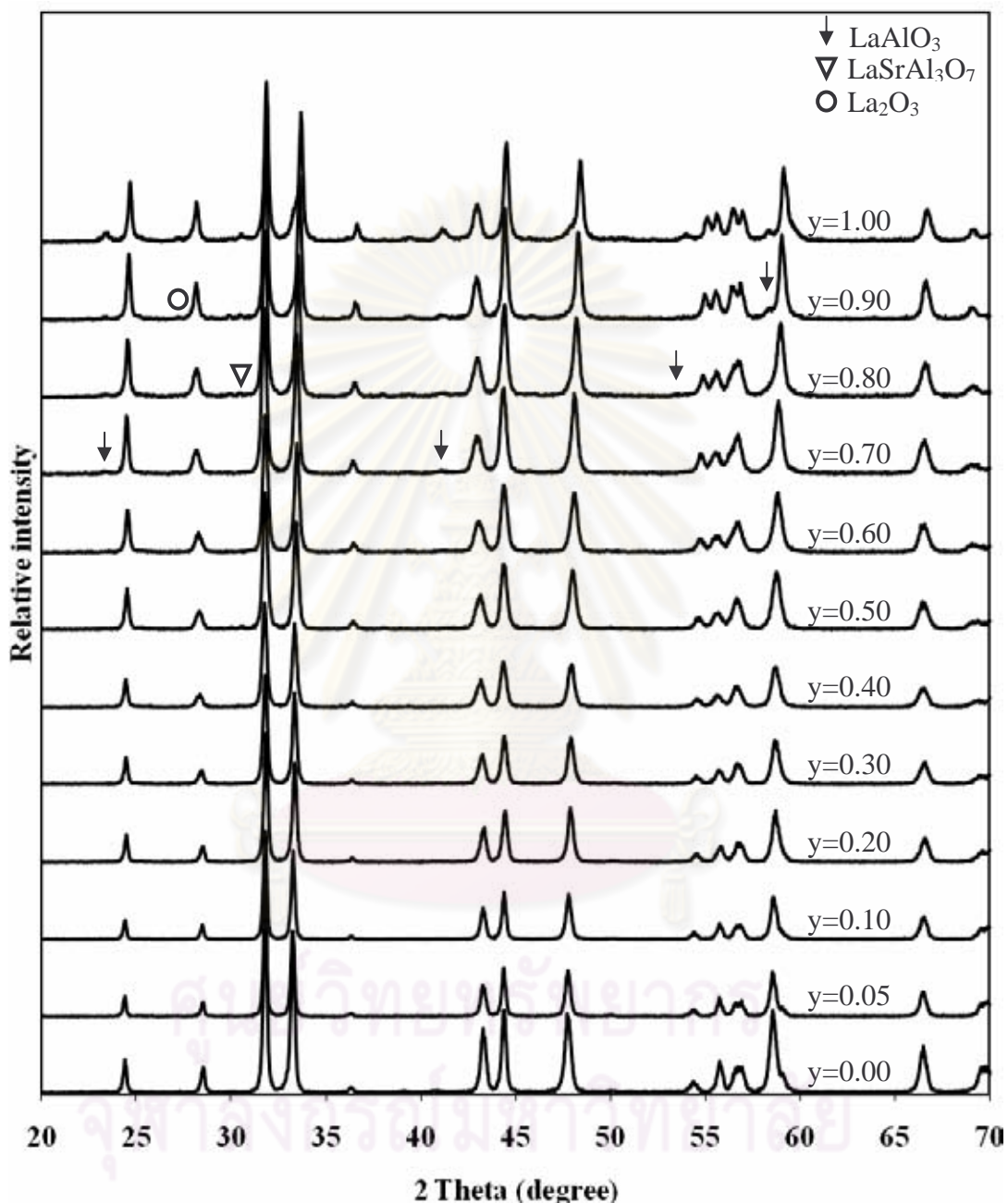
Figure 4.6 XRD patterns of $LaSrCo_{1-y}Al_yO_4$ (y = 0.0 – 1.0) calcined at 900°C for 5 h.

Next, the Al content was fixed at, 0.1 and the Sr contents were varied from 0.0 < x < 2.0. The calcination temperature was increased to 1100°C for better diffusion efficiency of metallic elements. The XRD patterns of $La_{1-x}Sr_xCo_{0.9}Al_{0.1}O_4$ are shown in figure 4.7 and 4.8. The XRD patterns indicated the desired single-phased

K$_2$NiF$_4$-typed samples were obtained for x = 0.8, 0.9, 1.0 and 1.2. The impurity phases of samples were identified as Sr$_3$Co$_2$O$_{6.13}$ (JCPDS 83-0375), SrO(Al$_2$O$_3$)$_2$ (JCPDS 72-1252), Al2O3 (JCPDS 75-0785) and perovskite phase for $0.1 \leq x \leq 1.0$ and Sr$_9$(Al$_9$O$_{18}$) (JCPDS 79-1094), SrLa(AlO$_4$) (JCPDS 89-0257), La$_2$O$_3$ (JCPDS 74-2430) and perovskite phase for $1.0 \leq x \leq 1.9$. All results of synthesis powder K$_2$NiF$_4$-typed oxides were summarized in table 4.3.
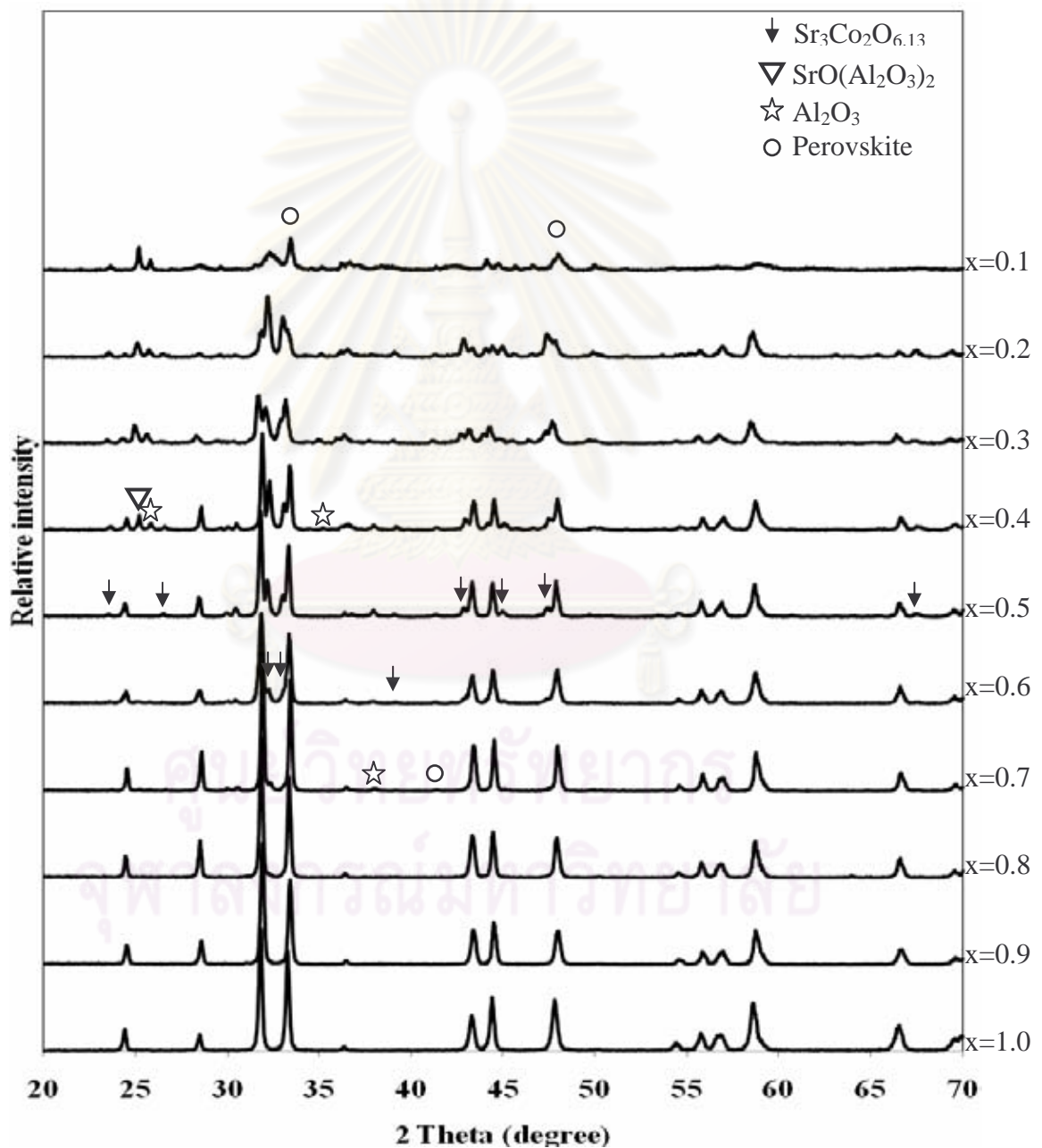
Figure 4.7 XRD patterns of La$_{2-x}$Sr$_x$Co$_{0.9}$Al$_{0.1}$O$_4$ (0.0 < x ≤ 1.0) calcined at 1100°C for 5 h.
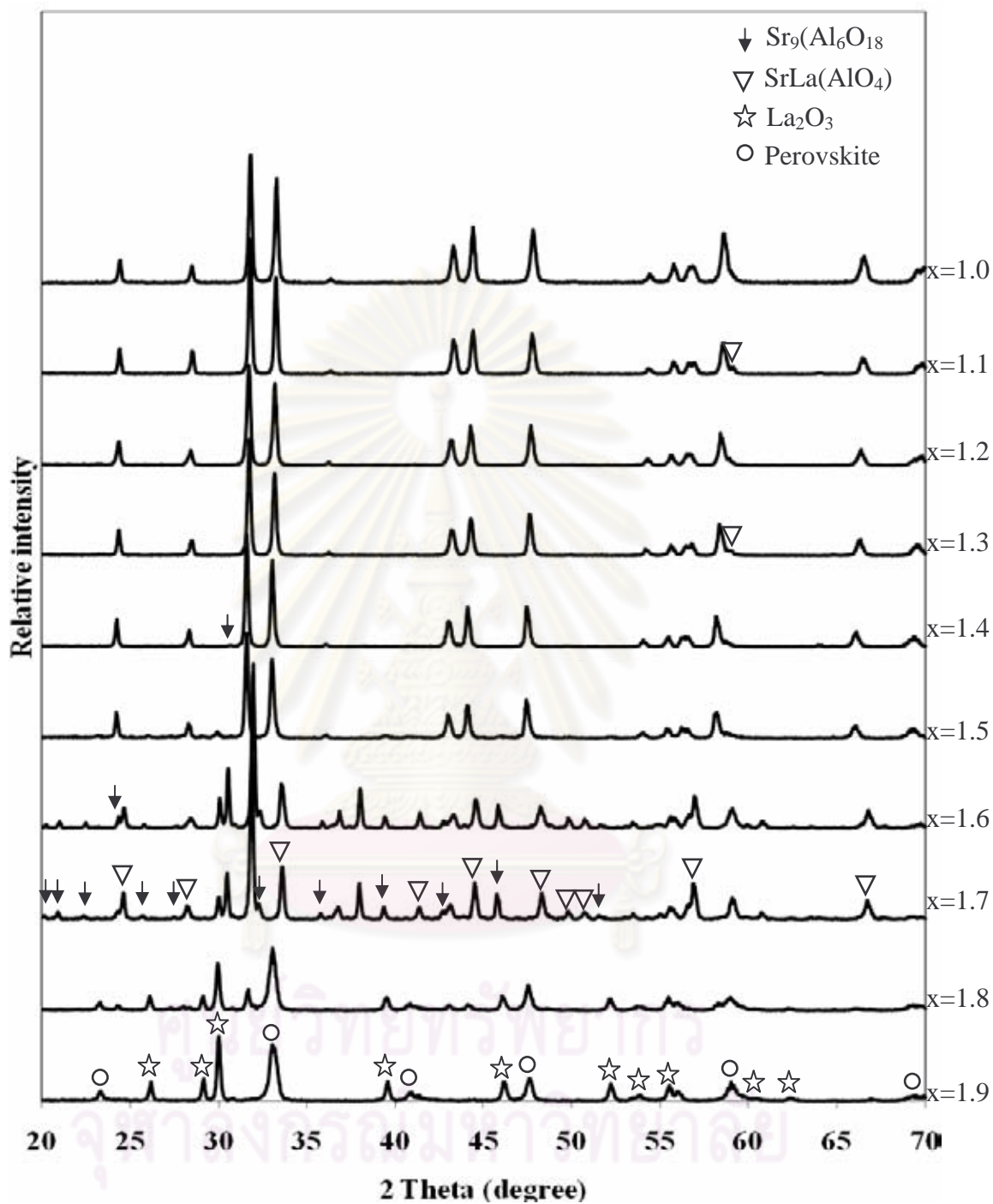
Figure 4.8 XRD patterns of $La_{2-x}Sr_xCo_{0.9}Al_{0.1}O_4$ ($1.0 \leq x < 2.0$) calcined at 1100°C for 5 h.

Table 4.3 The summary of single-phased K_2NiF_4-typed oxides ($La_{2-x}Sr_xCo_{1-y}Al_yO_4$)

		Al											
		1.0	0.9	0.8	0.7	0.6	0.5	0.4	0.3	0.2	0.1	0.05	0.0
	2.0												
	1.9												
	1.8												
	1.7												
	1.6												
	1.5												
	1.4												
	1.3												
	1.2										+		
	1.1												
Sr	1.0					+	+	+	+	+	+	+	+
	0.9										+		
	0.8										+		
	0.7												
	0.6												
	0.5												
	0.4												
	0.3												
	0.2												
	0.1												
	0.0												

+ is single-phased K_2NiF_4-typed oxide.

The $La_{1.0}Sr_{1.0}Co_{1-y}Al_yO_4$ (y = 0.0 – 0.6) series were chosen in order to investigate the effect of Al doping towards lattice parameters *a*, *b*, and *c*, unit cell volume and density. The XRD patterns of $La_{1.0}Sr_{1.0}Co_{1-y}Al_yO_4$ (y = 0.0 – 0.6) are shown in figure 4.8. It is clearly seen the shifts of strong peaks, indicating the change in unit cell parameters. Relationship of changing position of peak, that is changing 2θ, and lattice parameter could be explained by Bragg's law (equation 4.1) [34].

$$n\lambda = 2d \sin \theta \qquad (4.1)$$

From equation 4.1, when $n\lambda$ is constant, $\sin \theta$ relates to $\frac{1}{d}$.

$$\sin \theta \propto \frac{1}{d} \qquad (4.2)$$

For the tetragonal system, the relationship between *d*, lattice parameters *a* and *c* and Miller indices (*hkl*) are shown in equation 4.3.

$$\frac{1}{d^2} = \frac{h^2 + k^2}{a^2} + \frac{l^2}{c^2} \qquad (4.3)$$

Hence, $\qquad\qquad\qquad d \propto a$ when $\frac{l^2}{c^2}$ is zero $\qquad (4.4)$

and $\qquad\qquad\qquad d \propto c$ when $\frac{h^2 + k^2}{a^2}$ is zero $\qquad (4.5)$

Therefore; (*hk0*) $\qquad d \propto a$ that is $\sin \theta \propto \frac{1}{a} \qquad (4.6)$

(*00l*) $\qquad\qquad d \propto c$ that is $\sin \theta \propto \frac{1}{c} \qquad (4.7)$
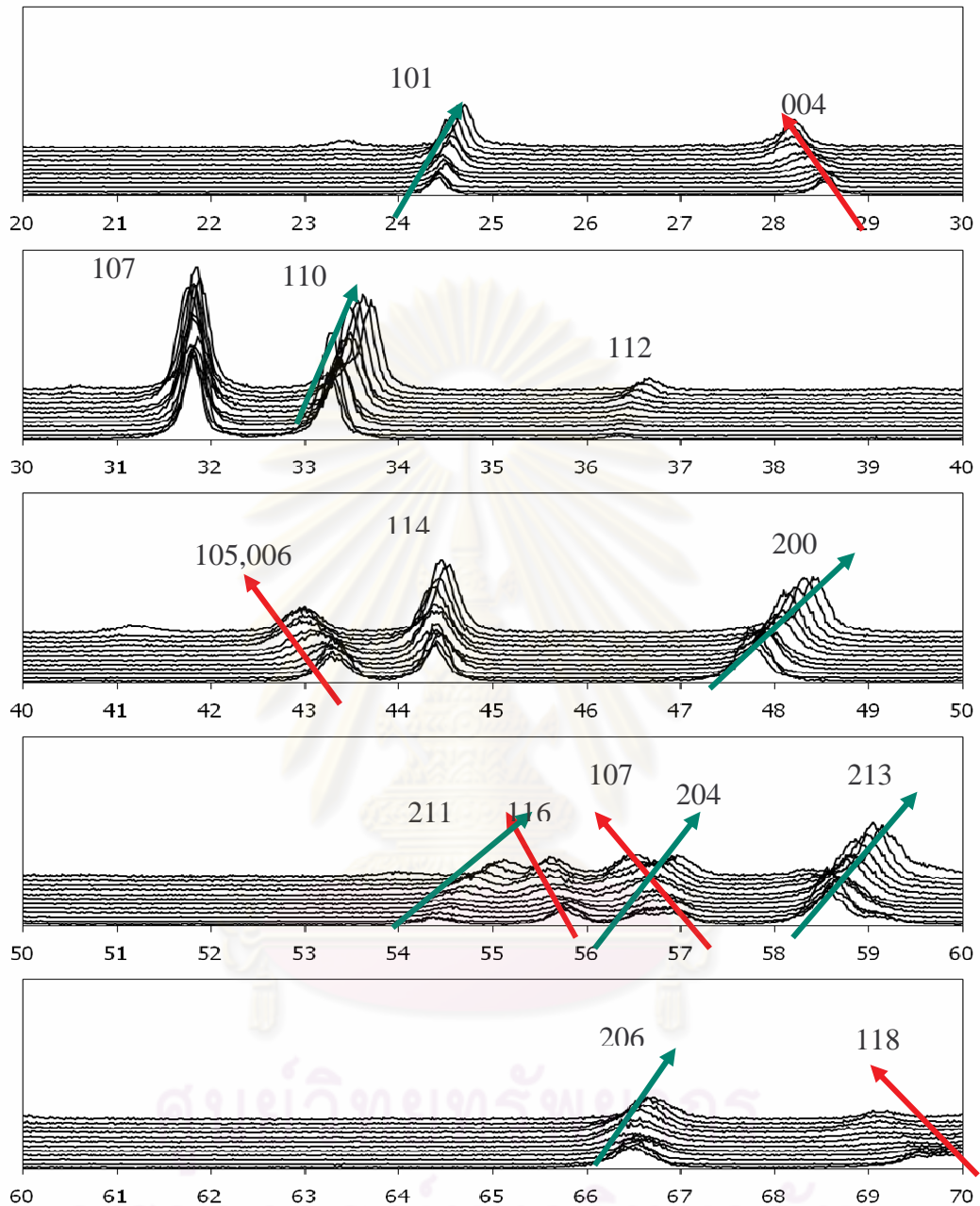
Figure 4.9 XRD patterns of K_2NiF_4-typed oxides $La_{1.0}Sr_{1.0}Co_{1-y}Al_yO_4$ (y = 0.0 – 1.0) calcined at 900°C for 5 h.

From figure 4.9, the increase of 2θ of the (*hk0*) planes with Miller indices (*200*) and (*110*) as a result of increasing Al content indicates the decrease in a parameter *a*. The decrease of 2θ of the (*00l*) planes at the Miller indices (*004*) and (*006*) as a result of increasing Al content indicates the increase in parameter *c*.

The patterns were indexed as the tetragonal structure ($a = b \neq c$ and $\alpha = \beta = \gamma = 90°$), and the lattice parameters were calculated from d spacings of strong peaks ((*101*), (*107*), (*110*), (*200*), (*114*) and (*200*)). The lattice parameters, unit cell volumes and densities calculated from the XRD patterns were summarized in table 4.4 and 4.5. Figure 4.10 reveals the trends of lattice parameters and unit cell volume upon Al contents. Lattice parameters calculated from the whole patterns have the same tendencies of the shifts of individual peaks in XRD profile that a decreases with increasing Al content. This could be explained in the same way as the change of a in LSCA perovskites that the substitution of the smaller cationic size of Al^{3+} (0.535Å) compared to Co^{3+} (0.545Å) in a B-site octahedral holes reduces the lattice parameter a in the perovskite layer of K_2NiF_4 structure. As a consequence, the increase in lattice parameter c with increasing Al content occurs in order to reduce the strain of the unit cell. Because of the opposite changes in two lattice parameters, the change of unit cell volume upon Al content is not significant. Density of samples decreases with increasing Al content because of the lighter weight of Al atom compared to Co atom, similar to what was discussed for perovskites.

Table 4.4 Lattice parameters and unit cell volumes of $LaSrCo_{1-y}Al_yO_4$ (y = 0.0 – 0.6)

Materials	Symmetry	a (Å)	c (Å)	Unit cell volume (Å^3)
$LaSrCoO_4$	Tetragonal	3.8070	12.4852	180.95
$LaSrCo_{0.95}Al_{0.05}O_4$	Tetragonal	3.8069	12.5129	181.34
$LaSrCo_{0.9}Al_{0.1}O_4$	Tetragonal	3.8036	12.4924	180.73
$LaSrCo_{0.8}Al_{0.2}O_4$	Tetragonal	3.7961	12.4984	180.11
$LaSrCo_{0.7}Al_{0.3}O_4$	Tetragonal	3.7956	12.5313	180.53
$LaSrCo_{0.6}Al_{0.4}O_4$	Tetragonal	3.7942	12.5699	180.96
$LaSrCo_{0.5}Al_{0.5}O_4$	Tetragonal	3.7854	12.6083	180.67
$LaSrCo_{0.4}Al_{0.6}O_4$	Tetragonal	3.7834	12.6152	180.58

Table 4.5 Densities of LaSrCo$_{1-y}$Al$_y$O$_4$ series (y = 0.0 – 0.6)

Materials	Density (g/cm^3)	Relative density
LaSrCoO$_4$	5.574	86.94
LaSrCo$_{0.95}$Al$_{0.05}$O$_4$	5.655	88.70
LaSrCo$_{0.9}$Al$_{0.1}$O$_4$	5.228	82.16
LaSrCo$_{0.8}$Al$_{0.2}$O$_4$	5.010	79.46
LaSrCo$_{0.6}$Al$_{0.4}$O$_4$	4.925	79.69
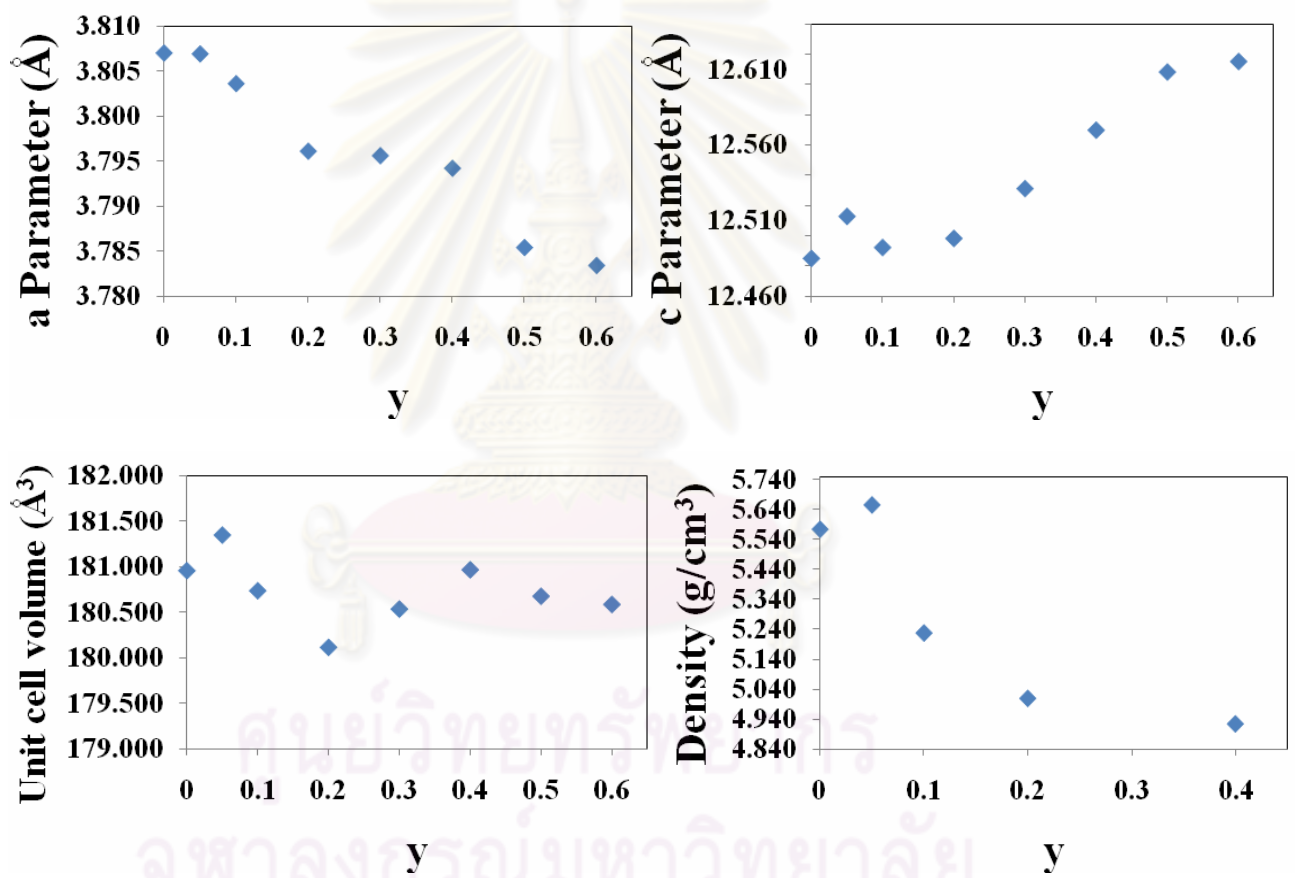
Figure 4.10 (a) Lattice parameters (b) unit cell volumes and (c) densities of K$_2$NiF$_4$ structure LaSrCo$_{1-y}$Al$_y$O$_3$ (y = 0.0 – 1.0).

4.1.2.2 Morphology of K_2NiF_4 – typed oxide

Figure 4.11 shows SEM images of K_2NiF_4-typed particles with different Al dopant levels. The decreasing tendency of particle size with increasing Al content of samples with y = 0.0 to 0.6 was observed. This may be explained as Al dopants introduce the strain to the structure, results to the discontinuous growth of particle. The particle sizes of $LaSrCo_{1-y}Al_yO_4$ (y = 0.0 - 0.6) are 0.26 µm, 0.21 µm, 0.17 µm, 0.16 µm, 0.14 µm and 0.11 µm respectively.
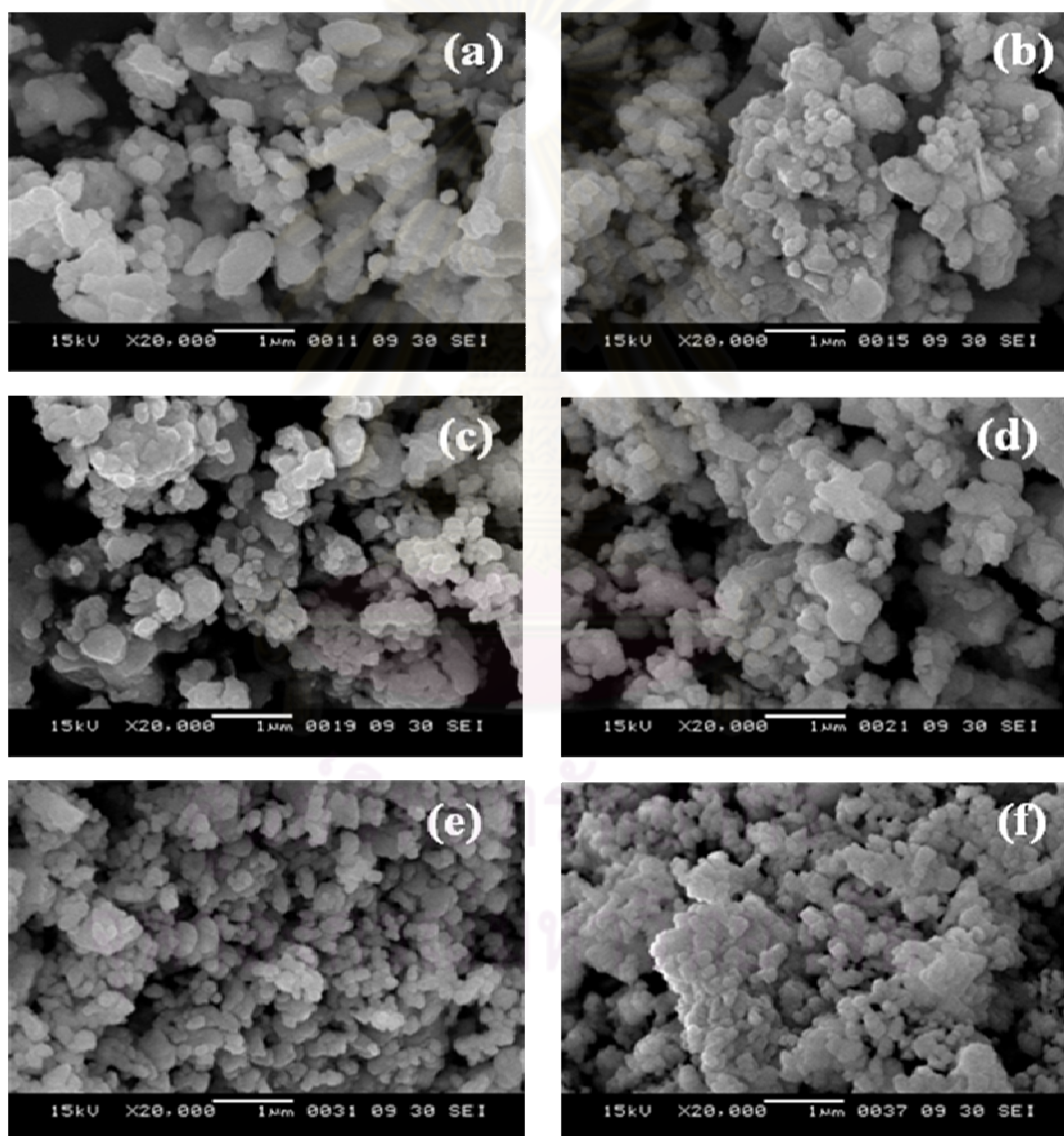

Figure 4.11 SEM images of (a) $LaSrCoO_4$, (b) $LaSrCo_{0.95}Al_{0.05}O_4$, (c) $LaSrCo_{0.9}Al_{0.1}O_4$, (d) $LaSrCo_{0.8}Al_{0.2}O_4$, (e) $LaSrCo_{0.6}Al_{0.4}O_4$, and (f) $LaSrCo_{0.4}Al_{0.6}O_4$ after calcination at 900°C for 5h.

4.2   Compatibility of LSCA with 8-YSZ electrolyte

4.2.1   The mixture of LSCA with 8-YSZ

The major problem in the use of cathode materials for SOFC is their reactivity with electrolyte materials, which leads to the formation of undesirable phases along the cathode – electrolyte interface. Generally these undesired phases are mixed metal oxides with less electrical conductivity and poor oxide permeability. For this reason, the study of possible reactions between synthesized LSCA and YSZ was investigated.

4.2.1.1 Perovskite materials

The chemical compatibility of all single-phased perovskites was investigated. The powder mixtures of perovskite samples and 8-YSZ in 50:50 weight ratios were ground and pressed in to pellets, then fired at selected temperatures. The fired pellets were characterized by XRD in order to identify the types of compounds formed at high-temperature operation. The $La_{0.6}Sr_{0.4}Co_{1-y}Al_yO_3$, y = 0.05, 0.1 and 0.2 were selected to observe the effect of Al contents, and their XRD patterns are shown in figures 4.12, 4.13, and 4.14 respectively. It was found that the undesired phase of $SrZrO_3$ (JCPDS 75-0465) started to appear since the firing temperature of 900°C, and $La_2Zr_2O_7$ (JCPDS 73-0444) did at 950°C.

The XRD patterns of $La_{0.6}Sr_{0.4}Co_{1-y}Al_yO_3$, y = 0.05, 0.1 and 0.2 fired at 900°C was zoomed between 30.6º – 31.2º 2θ in figure 4.15. The peak appeared in this range is the main peak of the undesired $SrZrO_3$ phase. The results show that this phase was formed less with the increase of Al content.
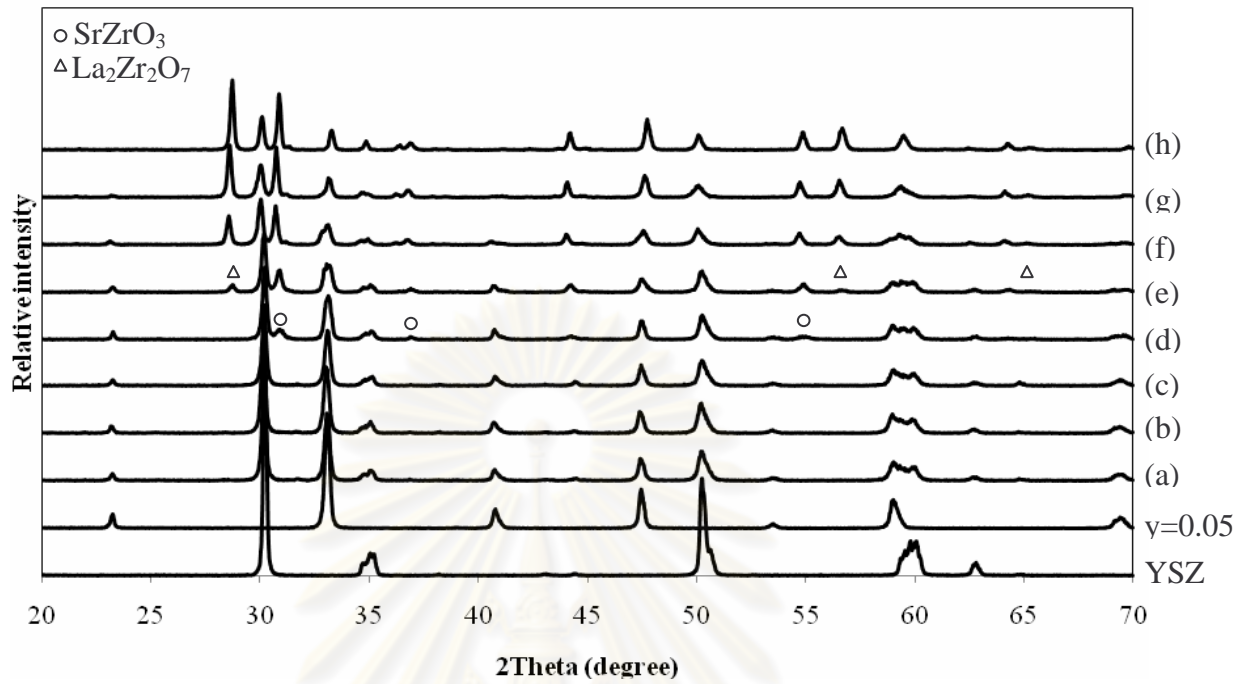
Figure 4.12 XRD patterns of mixed powder $La_{0.6}Sr_{0.4}Co_{0.95}Al_{0.05}O_3$ and 8-YSZ after firing at (a) 750°C, (b) 800°C, (c) 850°C, (d) 900°C, (e) 950°C, (f) 1000°C, (g) 1100°C and (h) 1200°C for 5 h.

Figure 4.13 XRD patterns of mixed powder $La_{0.6}Sr_{0.4}Co_{0.9}Al_{0.1}O_3$ and 8-YSZ after firing at (a) 750°C, (b) 800°C, (c) 850°C, (d) 900°C, (e) 950°C, (f) 1000°C, (g) 1100°C and (h) 1200°C for 5 h.

ศูนย์วิทยทรัพยากร
จุฬาลงกรณ์มหาวิทยาลัย
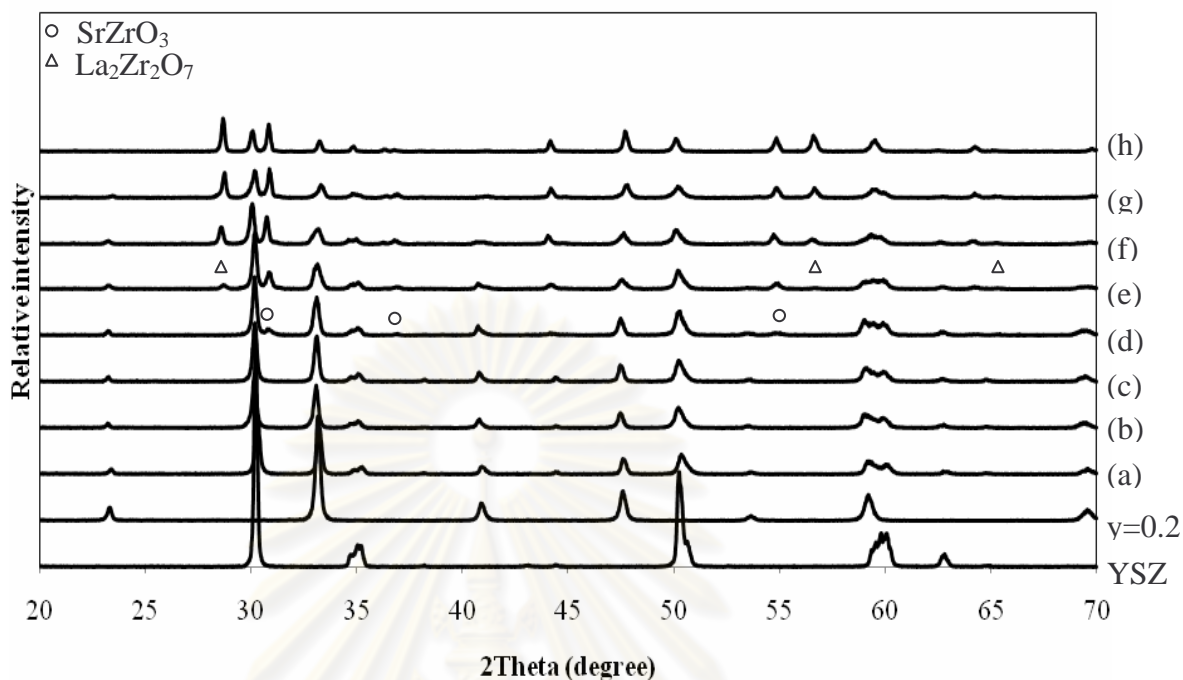
Figure 4.14 XRD patterns of mixed powder $La_{0.6}Sr_{0.4}Co_{0.8}Al_{0.2}O_3$ and 8-YSZ after firing at (a) 750°C, (b) 800°C, (c) 850°C, (d) 900°C, (e) 950°C, (f) 1000°C, (g) 1100°C and (h) 1200°C for 5 h.
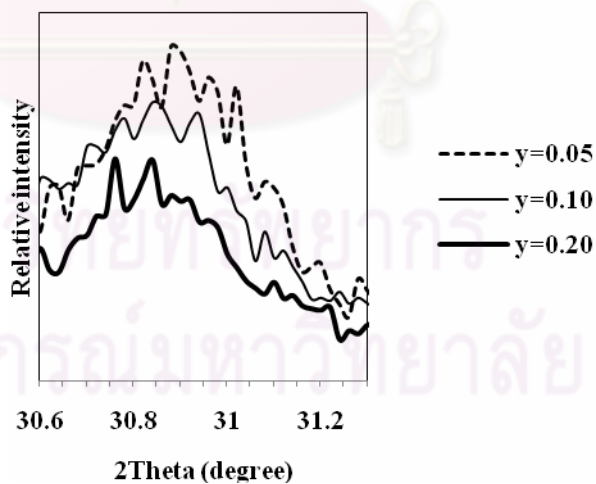
Figure 4.15 Relative intensities of the main peak of $SrZrO_3$ in the range of 30.6° – 31.2° 2θ as appeared in the XRD pattern of $La_{0.6}Sr_{0.4}Co_{1-y}Al_yO_3$ fired at 900°C for 5 h.

4.2.1.2 K$_2$NiF$_4$-typed LSCA

K$_2$NiF$_4$-typed samples were prepared in the similar manner as perovkite samples. The LaSrCo$_{1-y}$Al$_y$O$_4$, y = 0.05, 0.2, 0.4 and 0.6 were selected to observe the effect of Al contents, and their XRD patterns are shown in figure 4.16 – figure 4.19 respectively. It was found that the undesired phase of SrZrO$_3$, LaAlO$_3$ and the trace of LaCoO$_3$ started to appear at the firing temperature of 900°C.
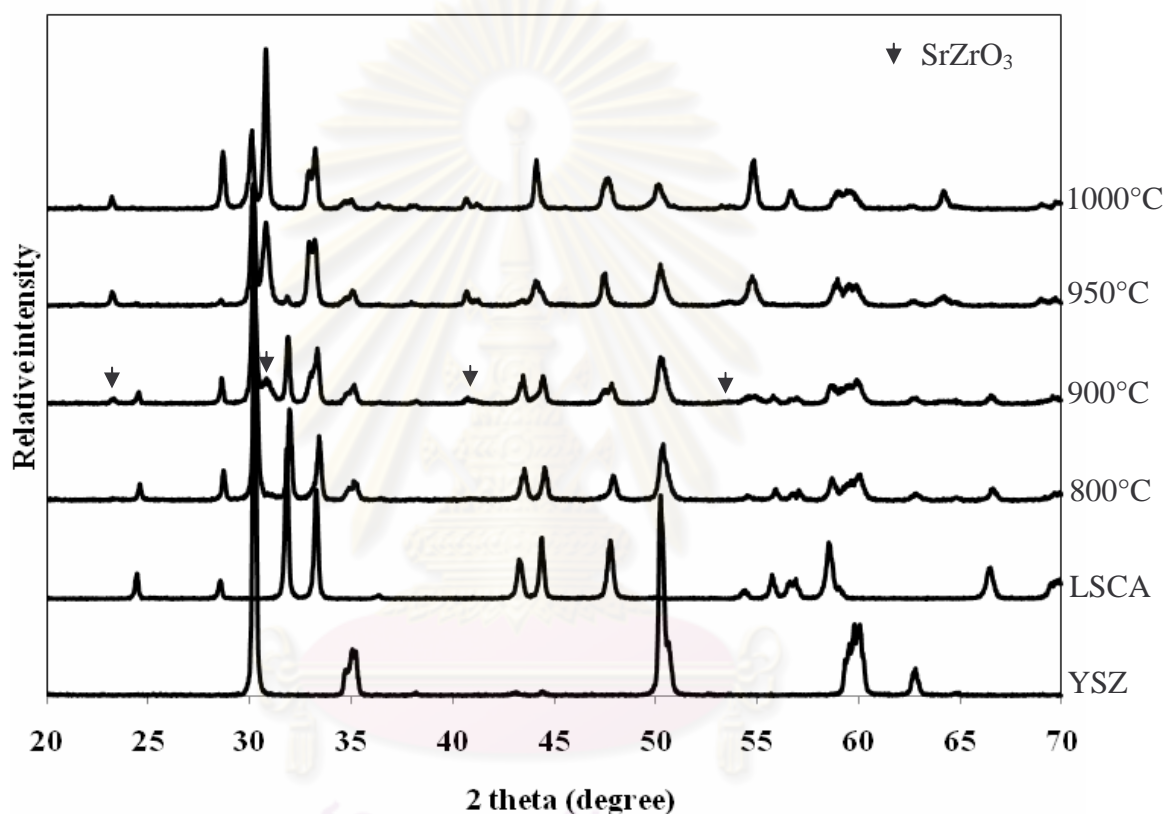
Figure 4.16 XRD patterns of mixed powder LaSrCo$_{0.95}$Al$_{0.05}$O$_4$ and 8-YSZ after firing at several temperatures for 5 h.
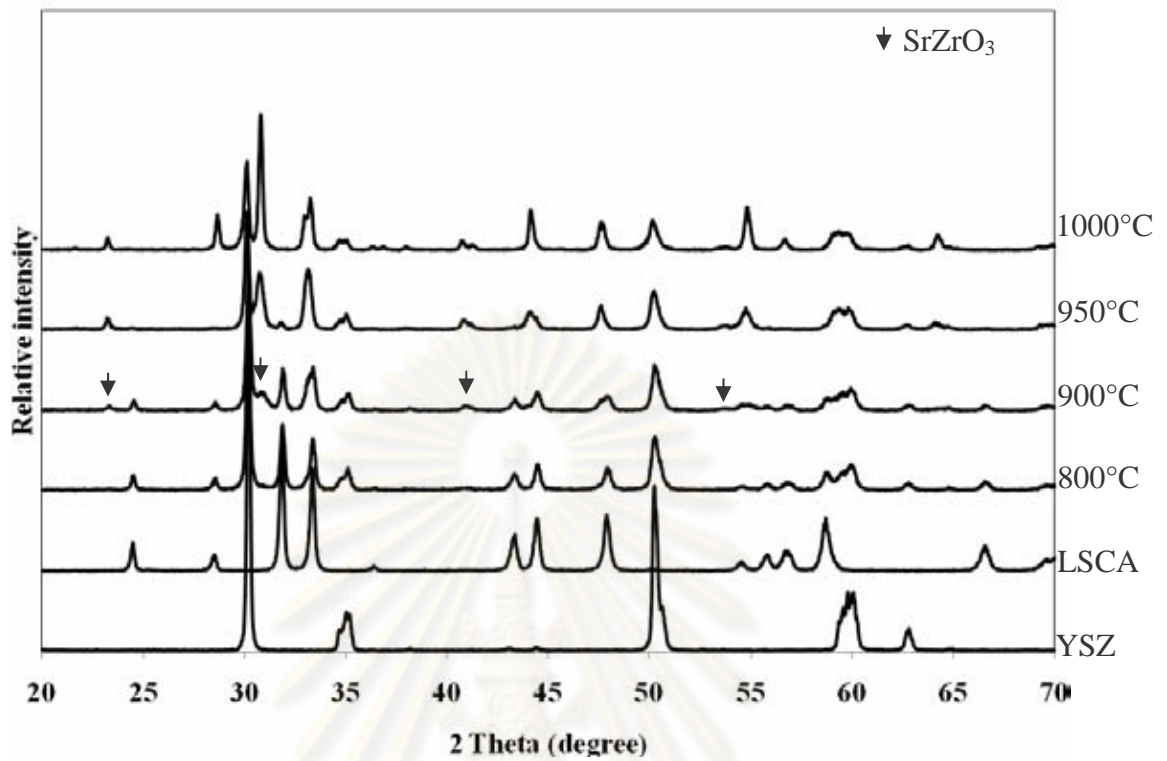
Figure 4.17 XRD patterns of mixed LaSrCo$_{0.8}$Al$_{0.2}$O$_4$ and 8-YSZ after firing at several temperatures for 5 h.

ศูนย์วิทยทรัพยากร
จุฬาลงกรณ์มหาวิทยาลัย
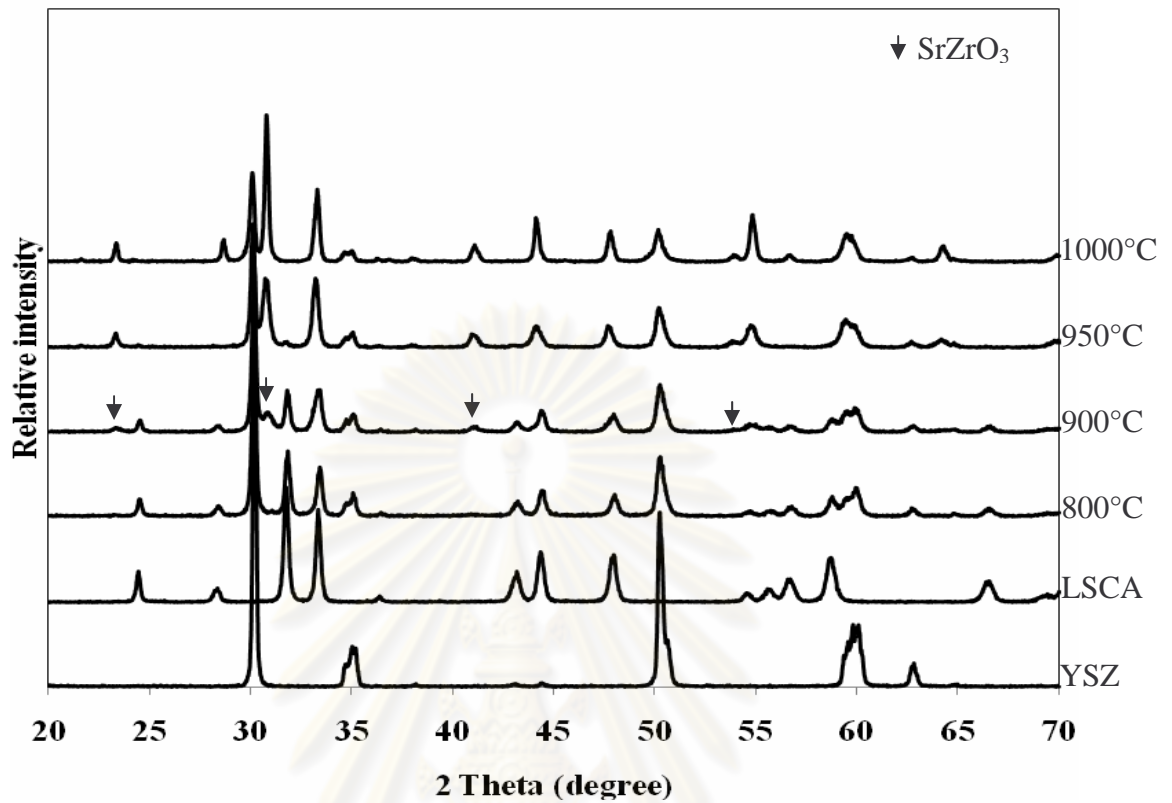
Figure 4.18   XRD patterns of mixed LaSrCo$_{0.6}$Al$_{0.4}$O$_4$ and 8-YSZ after firing at several temperatures for 5 h.
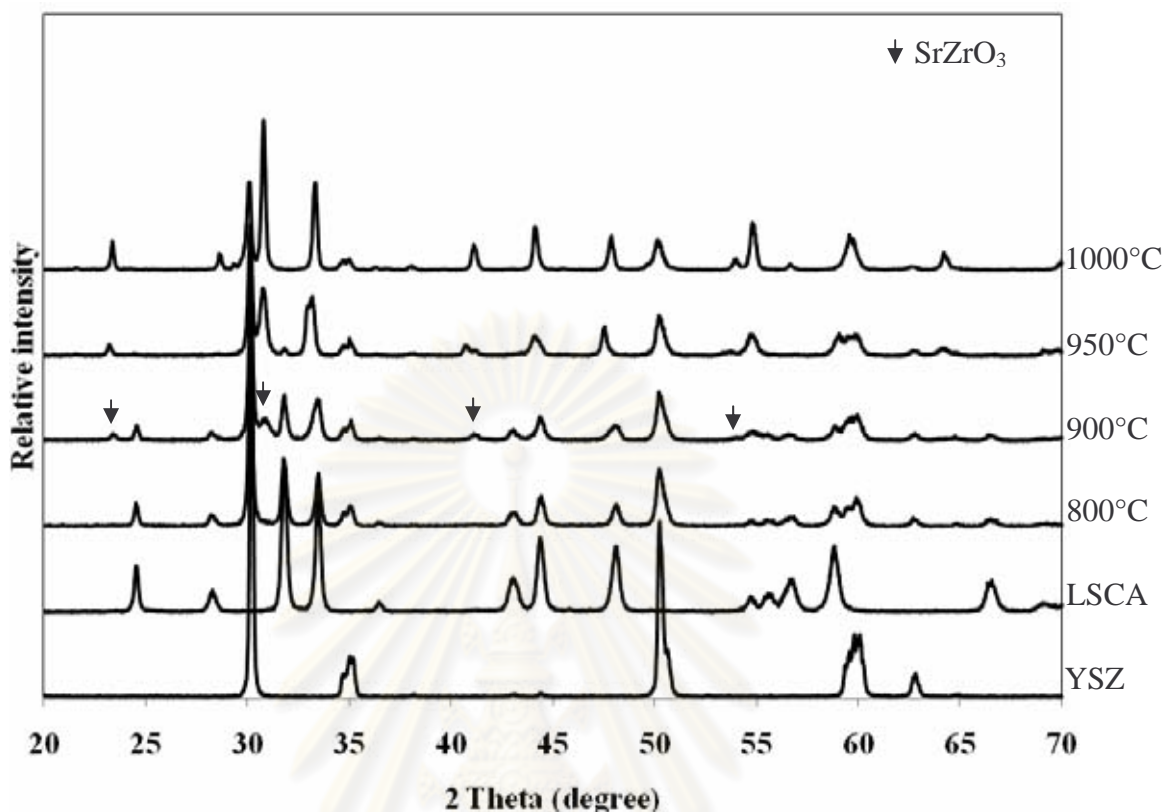
Figure 4.19 XRD patterns of mixed $LaSrCo_{0.4}Al_{0.6}O_4$ and 8-YSZ after firing at several temperatures for 5 h.

4.2.2 The membrane of LSCA powder with 8-YSZ

4.2.2.1 Perovskites

The chemical compatibilities from XRD results were confirmed by SEM/EDX. Figures 4.20 and 4.21 show the diffusion of metal cations, zirconium, lanthanum, strontium, cobalt and aluminum, at the interface of LSCA/YSZ. Figure 4.20 is the cross-sections of pellet samples showing the interface region around perovskite side and YSZ side. Three points were chosen in order to observe the diffusion of metals. The first point and second point are on the YSZ side and the other metals, La, Sr, Co and Al from LSCA would not be found. Likewise, Y and Zr would not be found at the third point in the LSCA region. For example, in figure 4.20 (a) y axis is the amount of metals, x axis is the point position on the membrane, point position 1, 2 on the YSZ side, and 3 on the LSCA side and each color of a bar represent the type of metals. In the case of perovskite, no zirconium diffused from the

electrolyte into the LSCA cathode. Similarly, the diffusion of lanthanum, strontium, cobalt and aluminum was not detected in the electrolyte part.
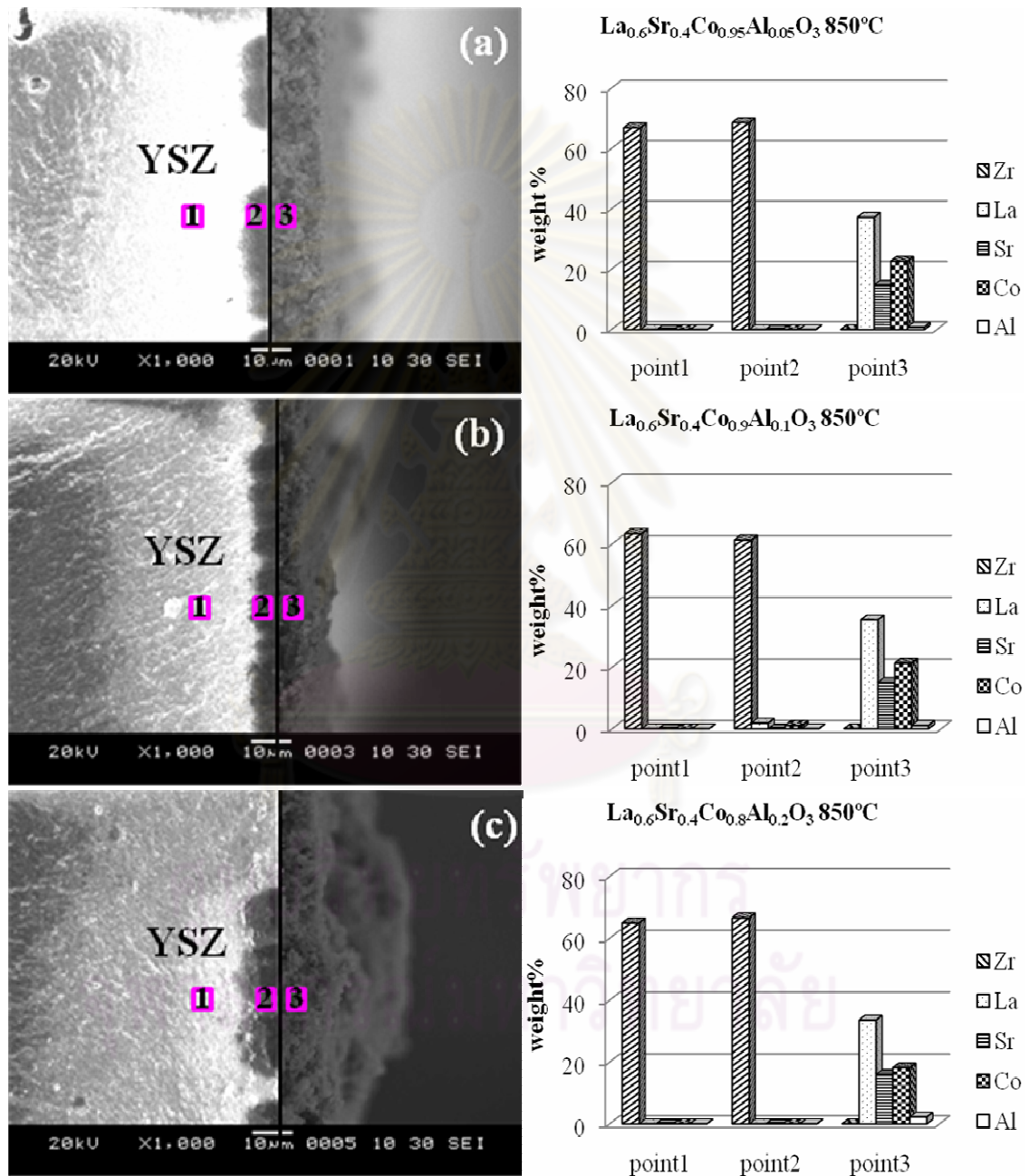
Figure 4.20 SEM images identified by Point EDX technique of (a) $La_{0.6}Sr_{0.4}Co_{0.95}Al_{0.05}O_3$, $La_{0.6}Sr_{0.4}Co_{0.9}Al_{0.1}O_3$ and $La_{0.6}Sr_{0.4}Co_{0.8}Al_{0.2}O_3$ after firing at 850°C for 5 h.

4.2.2.2 K_2NiF_4-typed oxides

In the case of K_2NiF_4-typed oxide materials, cations diffusion from electrolyte into the cathode was found after firing at 850°C, shown in figure 4.21. Metals from LSCA were not found at the 1 point inside YSZ pellet, but appeared significantly at YSZ side near the interface (point 2). Zr atoms from YSZ diffused into LSCA side significantly, but the diffused amount was less as the Al content in LSCA increase, indicating the role of Al in preventing the diffuse of Zr.
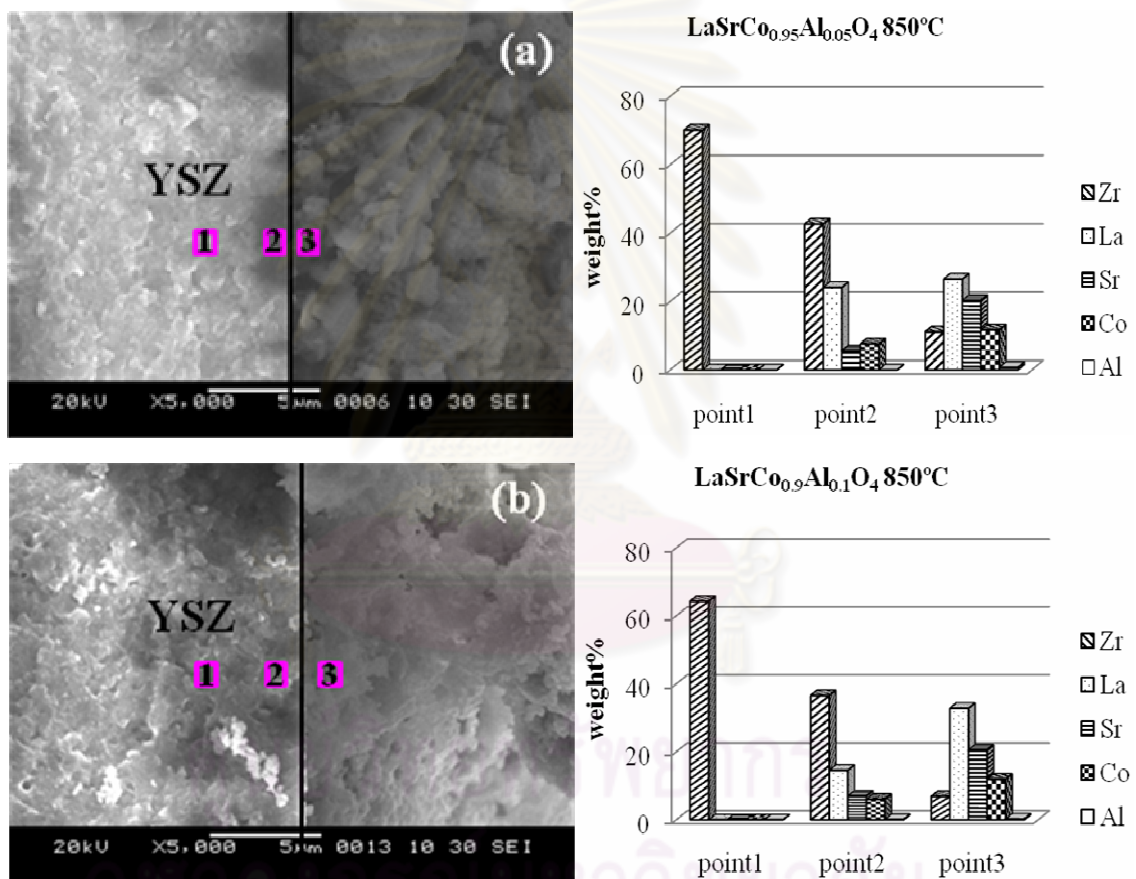
Figure 4.21 SEM images identified by Point EDX technique of (a) $LaSrCo_{0.95}Al_{0.05}O_4$ and (b) $LaSrCo_{0.91}Al_{0.1}O_4$ after firing at 850°C for 5 h.
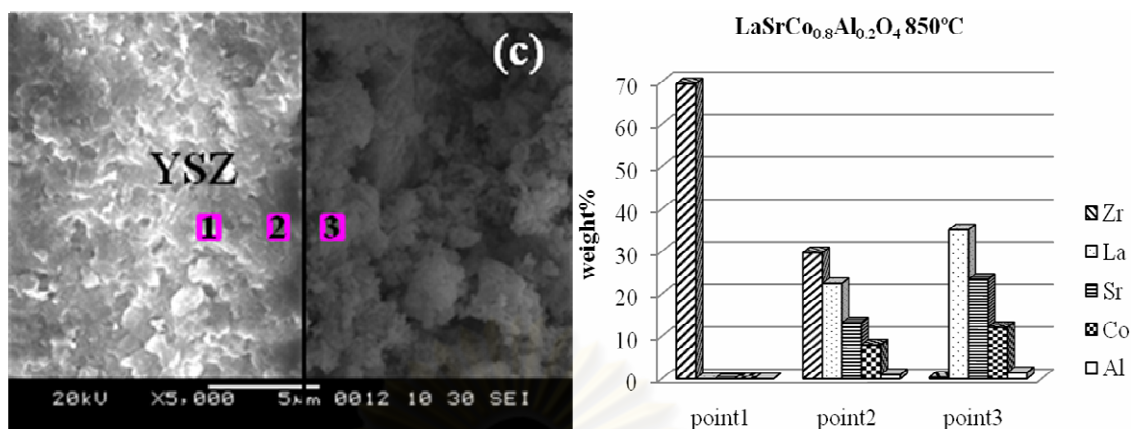
Figure 4.21 (continued) SEM images identified by Point EDX technique of (c) LaSrCo$_{0.8}$Al$_{0.2}$O$_4$ after firing at 850°C for 5 h.

4.2.3 Thermal expansion coefficients of LSCA

Thermal expansion of LSCA and YSZ should be matched because SOFCs operate at high temperature where most materials expand significantly. The mismatch would cause the breakdown of cell or shut down process. Results of thermal expansion coefficient were received by the dilatometer model NETZSCH DIL 402C.

The La$_{0.6}$Sr$_{0.4}$Co$_{1-y}$Al$_y$O$_3$ (perovskite) series and LaSrCo$_{1-y}$Al$_y$O$_4$ (K$_2$NiF$_4$ structure) series (y = 0.0, 0.05 and 0.2) were selected to study on the effect of Al to thermal expansion coefficients. Figure 4.22 and 4.24 show thermal expansion behaviors of perovskite series La$_{0.6}$Sr$_{0.4}$Co$_{1-y}$Al$_y$O$_3$ and K$_2$NiF$_4$-type oxide series LaSrCo$_{1-y}$Al$_y$O$_4$ respectively, compared to that of YSZ. The thermal expansion coefficient (TEC) was calculated from a slope at each temperature. The TEC values from room temperature up to 800°C of all materials are summarized in table 4.6.

For perovskite oxides, TECs decrease with increasing Al content because at high temperature Co ions change their magnetic state, Co^{+3} (and Co^{+2}), from low spin state to intermediate spin state. One electron of 3d^6 of three full-occupied t$_{2g}$ levels (3d^6 (t$_{2g}^6$ e$_g^0$)) moves to e$_g$ levels (3d^6 (t$_{2g}^5$ e$_g^1$)). In octahedral hole of cubic perovskites, oxygen and Co are overlapped by using σ bond and π bond as shown in figure 4.23. The σ bond results from the overlap between occupied p$_σ$ (O) and unoccupied e$_g$ (B). In the case of Co ions in B-site, the electron that is promoted to e$_g$ at high temperature would resides in the σ – antibonding level, and reduce the

strength of σ bond, leading to an expansion of the octahedral holes and therefore the crystal lattice. In other words, the electron in e_g repulses with the electrons in p_σ of oxygen atoms as shown in figure 4.23. Because Al has no d electron, the substitution of Co with Al reduces the number of coulombic repulsion at high temperature and then reduces the expansion [42]. The ideal graph should be linear but the experimental graph represents a nonlinear phenomenon that the change of slope is observed around 600ºC. This phenomenon is resulted by thermal lag (the slow thermal transfer) within the sample pellets under 600ºC [20].
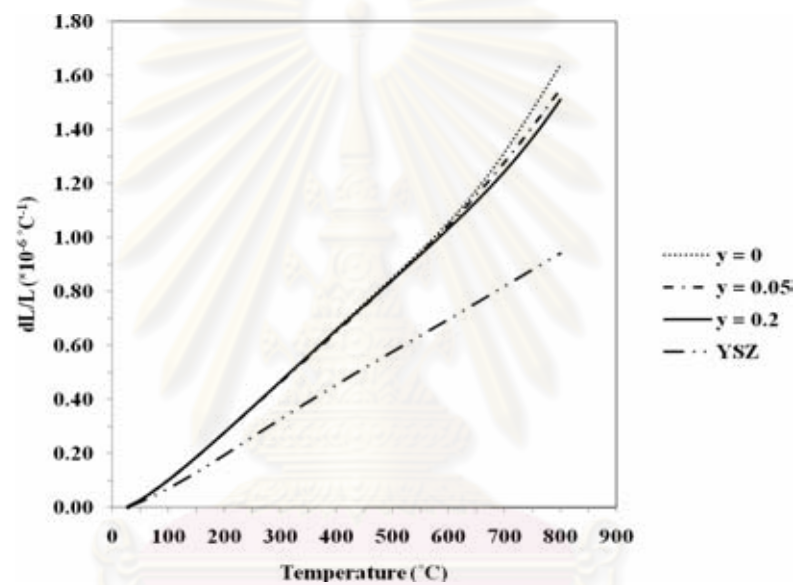
Figure 4.22 Thermal expansion of perovskite series $La_{0.6}Sr_{0.4}Co_{1-y}Al_yO_3$ and YSZ.
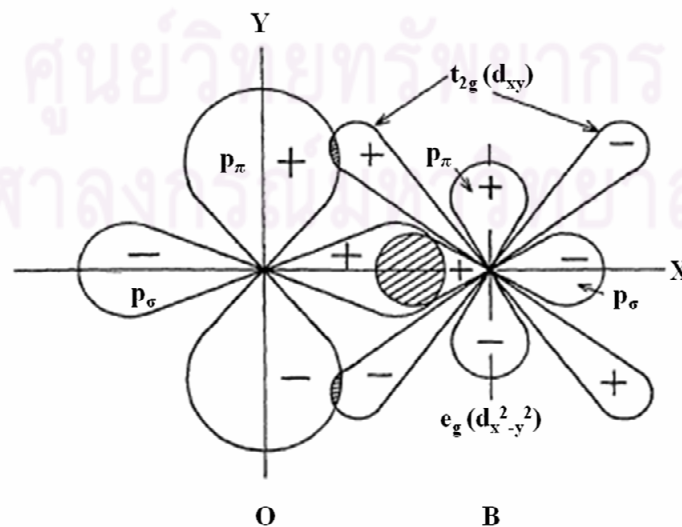
Figure 4.23 Covalent bond between oxygen ion and B-cations [21].
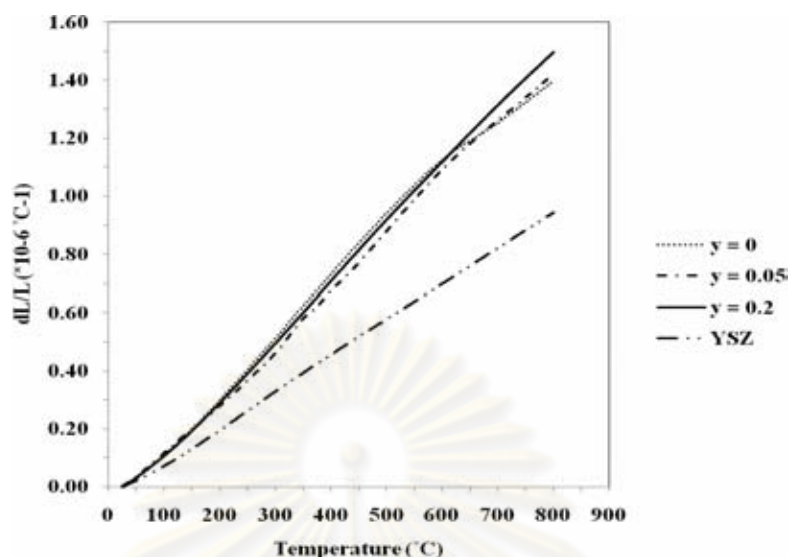
Figure 4.24   Thermal expansion of K_2NiF_4-typed oxide series $LaSrCo_{1-y}Al_yO_4$ and YSZ.

For K_2NiF_4-typed oxides, TEC values increase with increasing Al content. Although K_2NiF_4-typed oxides contains perovskite layer in its structure but it also contains rock salt layer in between, so that the TEC of this system could not be explained as in the case of LSCA perovskite. The increase of TECs with increasing Al content may relate to the smaller particle size of the samples with higher Al contents. The sample pellet may be denser when it has smaller particle size, and the expansion could be more evident.

Table 4.6   Thermal expansion coefficients of LSCA and YSZ

Materials	TEC ($\times 10^{-6}$ $°C^{-1}$)	References
$La_{0.6}Sr_{0.4}CoO_3$	21.5	This thesis
	20.5	[43]
$La_{0.6}Sr_{0.4}Co_{0.95}Al_{0.05}O_3$	20.3	This thesis
$La_{0.6}Sr_{0.4}Co_{0.8}Al_{0.2}O_3$	19.8	This thesis
$LaSrCoO_4$	18.2	This thesis
	14.3	[44]
$LaSrCo_{0.95}Al_{0.05}O_4$	18.4	This thesis
$LaSrCo_{0.8}Al_{0.2}O_4$	19.5	This thesis
YSZ	12.3	This thesis
	10.5	[45]

CHAPTER V
CONCLUSION AND SUGGESTION

5.1 Conclusion

Perovskite structure

The single phased $La_{1-x}Sr_xCo_{1-y}Al_yO_3$ perovskites with x = 0.0 – 1.0 and y = 0.0 – 0.2 were synthesized by the modified nitric citrate method with the calcination temperature of 900 – 1000°C for 5h. The minor phases were found in three samples when x = 0.5 – 0.7, y = 0.2. The crystal structure of all obtained single phased perovskites is cubic. The effect of Al doping was investigated using the $La_{0.6}Sr_{0.4}Co_{1-y}Al_yO_3$ (y = 0.0, 0.05, 0.1 and 0.2) series as a representative. The unit cell volume, a lattice parameter (*a*), density and particle size decrease with the increase of Al content because the smaller cationic size of Al^{3+} (0.535Å) substituted in Co^{3+} (0.545Å) sites.

K_2NiF_4-typed structure

The single phase of K_2NiF_4-typed $La_{2-x}Sr_xCo_{1-y}Al_yO_4$ were obtained when x = 0.8 – 1.2 (except x = 1.1), y = 0.1 and when x = 1.0, y = 0.0 – 0.6 by the modified nitric citrate method. The calcination was at 900-1100°C for 5h. The crystal structure of all single phased K_2NiF_4-typed structure is tetragonal. The effect of Al doping was investigated using the $LaSrCo_{1-y}Al_yO_4$ (y = 0.0 – 0.6) series as a representative. With the increase of Al content, the lattice parameter a decreases, while the lattice parameter c increases. The density and particle size also decreases as Al content increases.

Chemical compatibility of both structures with 8-YSZ

The chemical compatibilities of $La_{0.6}Sr_{0.4}Co_{1-y}Al_yO_3$ (y = 0.05, 0.1 and 0.2) and $LaSrCo_{1-y}Al_yO_4$ (y = 0.05, 0.2, 0.4 and 0.6) with 8-YSZ were investigated by observing the XRD patterns of their powder mixtures at the temperatures of 750°C to 1200°C and 800°C to 1000°C respectively.

    a. Perovskites showed the good compatibility with 8-YSZ from room temperature up to 850°C. The undesired phases of $SrZrO_3$ and

$La_2Zr_2O_7$ were found since the temperatures of 900°C and 950°C respectively. The amount of $SrZrO_3$ decreases with increases Al content.

b. K_2NiF_4-typed oxides showed the good compatibility with 8-YSZ from room temperature up to 850°C The undesired $La_2Zr_2O_7$ was found at higher temperature.

The powder XRD results were confirmed by the SEM/EDX results of the membrane interface between oxides and 8-YSZ. The diffusion of metal atoms across the interface were not found for perovskite/YSZ after fired at 850ºC but it was detected for K_2NiF_4/YSZ after fired at 850ºC.

The thermal expansion coefficients of $La_{0.6}Sr_{0.4}Co_{1-y}Al_yO_3$ (y = 0.0, 0.05 and 0.2) decrease with the increase of Al content. While the thermal expansion coefficients of $LaSrCo_{1-y}Al_yO_4$ (y = 0.0, 0.05 and 0.2) increase with the increase of Al content.

5.2   Suggestion

In order to regard the Al doped $La_{1-x}Sr_xCoO_3$ and Al doped $La_{2-x}Sr_xCoO_4$ series as the candidates of a cathode material for SOFC, the electronic conductivities must be measured because Al may decrease the electronic conductivity of the materials. Although Al may decrease the electronic conductivity but Al doped $La_{1-x}Sr_xCoO_3$ has much enough electronic conductivity to be the cathode for SOFC.

REFERENCES

[1]   World primary energy demand. Available from:
        http://www.eia.doe.gov/ [2010, February 25]

[2]   Global carbon cycle. Available from:
        http://www.eia.doe.gov/environment.html [2010, February 25]

[3]   Bevilacqua, M.; Montini, T.; Tavagnacco, C.; Vicario, G.; Fornasiero, P.;
        Graziani, M. Influence of synthesis route on morphology and electrical
        properties of $LaNi_{0.6}Fe_{0.4}O_3$. *Solid State Ionics* 177 (2006): 2957-2965.

[4]   Kharton, V.V.; Viskup, A.P.; Kovalevsky, A.V.; Naumovich, E.N.; Marques,
        F.M.B. Ionic transport in oxygen-hyperstoichiometric phases with
        K_2NiF_4-type structure. *Solid State Ionics* 143 (2001): 337–353.

[5]   Sahu, A.K.; Ghosh, A.; Suri, A.K.; Sengupta, P.; Bhanumurthy, K. Studies on
        chemical compatibility of lanthanum strontium manganite with yttria-
        stabilized zirconia. *Mater. Lett.* 58 (2004): 332–3336.

[6]   Munnings, C.N.; Skinner, S.J.; Amow,G.; Whifield, P.S.; Davidson, I.J.
        Structure, stability and electrical properties of the $La_{(2-X)}Sr_XMnO_{4\pm\delta.}$
        solid solution series. *Solid State Ionics* 177 (2006): 1849-1853.

[7]   Yamamoto, O., Takeda, Y., Kanno, R., Noda, N. Perovskite-type oxides as
        oxygen electrodes for high temperature oxide fuel cells. *Solid State
        Ionics* 22 (1987): 241 – 246.

[8]   Teraoka, Y., Npbunaga, T., Okamoto, K., Miura, N., Yamazoe, N. Influence of
        constituent metal cations in substituted $LaCoO_3$ on mixed conductivity
        and oxygen permeability. *Solid State Ionics* 48 (1991): 207 – 212.

[9]   Kostogloudis, G.C., Tsiniarakis, G., Ftikos, C. Chemical reactivity of
        perovskite oxide SOFC cathodes and Yttria stabilized zirconia. *Solid
        State Ionics* 135 (2000): 529 – 535.

[10]   Hrovat, M., Bernik, S., Kuščer, D., Holc, J., Kolar, D. Evaluation of the
        characteristics of $La(Co_{1-x}Al_x)O_3$ as possible SOFC cathodes. *J. Mater.
        Sci. Lett.* 17 (1998): 1957 – 1959.

[11]   Kajitani, M., Mastsuda, M., Miyake, M. Effect of doping on crystal structure
       and electrical conduction properties of $LaGa_{0.9}Mg_{0.1}O_{2.95}$ perovskite
       compound. *Solid State Ionics* 178 (2007): 355 – 358.

[12]   Marozau, I.P., Kharton, V.V., Viskup, A.P., Frade, J.R., Samakhval, V.V.
       Electronic conductivity, oxygen permeability and thermal expansion of
       $Sr_{0.7}Ce_{0.3}Mn_{1-x}Al_xO_3$. *J. Eur. Ceram. Soc.* 26 (2006): 1371 – 1378.

[13]   Iamsa-ard, S. Chemical and physical compatibility of lanthanum nickel iron
       oxides and yttria stabilized zirconia, M.Sc. Thesis, Petrochemistry and
       Polymer Science, Faculty of Science, Chulalongkorn University,
       Bangkok, 2007

[14]   Zhou, A.J., Zhu, T.J., Zhao, X.B. Thermoelectric properties of perovskite-type
       oxide $La_{1-x}Sr_xCoO_3$ (x = 0, 0.1) prepared by solid state reactions.
       Mater. Sci. Eng. B 128 (2006): 174 – 178.

[15]   Ahmad, A.L., Idrus, N.F., Othman, M.R. Preparation of perovskite alumina
       ceramic membrane using sol-gel method. *J. Membrane Sci.* 262
       (2005): 129 – 137.

[16]   Liu, Z., Han, M.F., Miao, W.T. Preparation and characterization of graded
       cathode $La_{0.6}Sr_{0.4}Co_{0.2}Fe_{0.8}O_{3-\delta}$. *J. Power Sources* 173 (2007): 837 –
       841.

[17]   Matsuura, T., Tabuchi, J., Mizusaki, J., Yamauchi, S., Fueki, K. Electrical
       properties of $La_{2-x}Sr_xCoO_4$: structure, electrical conductivity and
       seebeck coefficient of single crystals (x = 0.0, 0.5, 1.0 and 1.5). *J. Phys.
       Chem. Solids* 49 (1988): 1403 – 1408.

[18]   Vashook, V.V., Ullmannn, H., Olshevskaya, O.T., Kulik, V.P., Lukashevich,
       V.E., Kokhanovskij, L.V. Composition and electrical conductivity of
       some cobaltates of the type $La_{2-x}Sr_xCoO_{4.5-x/2\pm\delta}$. *Solid State Ionics* 138
       (2000): 99 – 104.

[19]   James, M., Tedesco, A., Cassidy, D., Colella, M., Smythe, P.J. The phase
       diagram and crystal chemistry of strontium-doped rare earth cobaltates:
       $Ln_{2-x}Sr_xCoO_{4+\delta}$ (Ln = La – Dy). *J. Alloy Compd.* 419 (2006): 201 –
       207.

[20]   Raj, E.S., Skinner, S.J., Kilner, J.A. Solution synthesis and electrical properties of K_2NiF_4-type $LaSrAlO_4$. *Solid State Sci.* 6 (2004): 825 – 829.

[21]   Richter, J., Holtappels, P., Graule, T., Nakamura, T., Gauckler, L.J. Materials design for perovskite SOFC cathodes. *Monatsh. Chem.* 140 (2009): 985 – 999.

[22]   Flat plate solid oxide fuel cells. Available from: http://www.doitpoms.ac.uk/tlplib/fuel-ells/figures/flat_plate_sofcsml. [2010, February 25]

[23]   Wandekar, R.V., Wani, B.N., Bharadwaj, S.R. Crystal structure, electrical conductivity, thermal expansion and compatibility studies of co-substituted lanthanum strontium manganite system. *Solid State Sci.* 11 (2009): 240 – 250.

[24]   Kamata, H., Hosaka, A. Chemical compatibility of perovskite-type oxide $La_{0.7}Ca_{0.3}Cr_{1-y}Co_yO_3$ with Y_2O_3 stabilized ZrO_2. *Mater. Res. Bull.* 30 (1995): 679 – 687.

[25]   Amesti, A.M., Larranaga, A., Martinez, L.M.R., Aguayo, A.T., Pizarro, J.L., No, M.L., Laresgoiti, A., Arriortua, M.I. Reactivity between $La(Sr)FeO_3$ cathod, doped CeO_2 interlayer and yttria-stabilized zirconia electrolyte for solid oxide fuel cell applications. *J. Power Sources* 185 (2008): 401 – 410.

[26]   Taroncón, A., Martínez, J.P., López, D.M., Morata, A., Morales, J.C.R., Núnez, P. Stability, chemical compatibility and electrochemical performance of $GdBaCo_2O_{5+x}$ layered perovskite as a cathode for intermediate temperature solid oxide fuel cells. *Solid State Ionics* 179 (2008): 2372 – 2378.

[27]   Parsons, I. *Fuel cell Handbook*, 5th ed., Morgantown, West Virginia, 2000.

[28]   Solid oxide fuel cell. Available from: www.mne.eng.psu.ac.th/fuelcell/Sofc2.jpg.[2010, February 25]

[29]   Vielstich, W., Gasteiger, H.A., Lamm, A. *Handbook of fuel cells – Fundamentals, Technology and Applications*, Wiley, New York, 2003.

[30] Ishihara, T., Matsuda, H., Takita, Y. Effects of rare earth cations doped for La site on the oxide ionic conductivity of LaGaO$_3$-based perovskite typed oxide. *Solid State Ionics* 79 (1995): 147 – 151.

[31] Feng, L.M., Jiang, L.Q., Zhu, M., Liu, H.B., Zhou, X., Li, C.H. Formability of ABO$_3$ cubic perovskites. *J. Phys. Chem. Solids* 69 (2008): 967 – 974.

[32] Jiang, L.Q., Guo, J.K., Liu, H.B., Zhu, M., Zhou, X., Wu, P., Li, C.H. Prediction of lattice constant in cubic perovskites. *J.Phys. Chem. Solids* 67 (2006): 1531 – 1536.

[33] Chen, B.H. Introduction of tolerance factor for the Nd$_2$CuO$_4$ (*T*´)-type structure. *J. Solid State Chem.* 125 (1996): 63 – 66.

[34] West, A.R. *Basic solid state chemistry*, 2nd ed., Wiley, Singapore, 1999.

[35] Akaratiwa, S. *Fundamentals of catalyst reaction engineering*, Top publishing, Bangkok, 2003.

[36] Daroukh, M.A.; Vashook, V.V.; Ullmann, H.; Tietz, F.; Raj, I.A. Oxides of the AMO$_3$ and A$_2$MO$_4$-type: structural stability, electrical conductivity and thermal expansion. *Solid State Ionics* 158 (2003): 141 – 150.

[37] L.E. Smart, E.A.Moore *Solid state chemistry: An introduction*, 3rd ed., CRC Press, USA, 2005.

[38] Archimedes' principle and specific density [2006]. Available from: http://www.physics.arizona.edu/physics2006. [2010, February 26]

[39] Kishimoto, H., Sakai, N., Horita, T., Yamaji, K. Interface reaction and cation transport behavior between perovskite oxides of La$_{1-x}$Sr$_x$CoO$_3$ and La$_{0.8}$Sr$_{0.2}$FeO$_3$. *Solid State Ionics* 179 (2008): 1338 – 1342.

[40] Rahaman, M.N. *Ceramic processing and sintering*, 2nd ed.,Marcel Dekker, New York, 1995.

[41] Dasgupta, N., Krishnamworthy, R., Jacob, K.T. Crystal structure, thermal expansion and electrical conductivity of Nd$_{0.7}$Sr$_{0.3}$Fe$_{1-x}$Co$_x$O$_3$ ($0 \leq x \leq 0.8$). *Mater. Sci. Eng. B* 90 (2002): 278 – 286.

[42] Uhlenbruck, S., Tietz, F. High-temperature thermal expansion and conductivity of cobaltites:potentials for adaptation of the thermal expansion to the demands for solid oxide fuel cells. *Mater. Sci. Eng. B* 107 (2004): 277 – 282.

[43]   Ullmann, H., Trofimenko, N., Tietz, F., Stover, D., Khanlou, A.A. Correlation
       between thermal expansion and oxide ion transport in mixed
       conducting perovskite-type oxides for SOFC cathodes. *Solid State
       Ionics* 138 (2000): 79 – 90.

[44]   Daroukh, N.L., Vashook, V.V., Ullmann, H., Tietz, F., Raj, I.A. Oxides of the
       AMO_3 and A_2MO_4-type: structural stability, electrical conductivity and
       thermal expansion. *Solid State Ionics* 158 (2003): 141 – 150.

[45]   Mori, M., Abe, T., Itoh, H., Yamamoto, O., Takeda, Y., Kawahara, T. Cubic-
       stabilized zirconia and alumina composites as electrolytes in planar
       type solid oxide fuel cells. *Solid State Ionics* 74 (1994): 157 – 164.

APPENDIX

The calculations for synthesis by the combustion method

The molecular weights of starting materials

Chemicals	Molecular weight	Metal	Molecular weight of metal
La(NO$_3$)$_3$.6H$_2$O	433.02	La	138.91
Sr(NO$_3$)$_2$	211.63	Sr	87.62
Co(NO$_3$)$_2$.6H$_2$O	291.03	Co	58.933
Al(NO$_3$)$_3$.9H$_2$O	387.5	Al	26.98
Citric acid	192.13	O	16.00

1.   Perovskite structure

<u>Example</u> Preparation of 1 g La$_{0.6}$Sr$_{0.4}$Co$_{0.9}$Al$_{0.1}$O$_3$ (LSCA6491)

Molecular weight of LSCA6491 = 222.162 g/mol

$$\text{LSCA6491} \qquad 222.162 \text{ g} \quad = 1 \text{ mol}$$

$$\text{LSCA6491} \qquad\qquad 1 \text{ g} \quad = 1 \text{ g}/222.162 \text{ g}$$

$$= 4.5012 \times 10^{-3} \text{ mol}$$

Calculation of La(NO$_3$)$_3$.6H$_2$O

LSCA6491   1 mol   =   La 0.6 mol

LSCA6491   4.5012 $\times$ 10^{-3} mol   =   0.6 $\times$ 4.5012 $\times$ 10^{-3} mol

=   2.7007 $\times$ 10^{-3} $\times$ 433.03 g

La   =   1.1695 g

Calculation of Sr(NO$_3$)$_2$

LSCA6491   1 mol   =   Sr 0.4 mol

LSCA6491   4.5012 $\times$ 10^{-3} mol   =   0.4 $\times$ 4.5012 $\times$ 10^{-3} mol

=   1.800 $\times$ 10^{-3} $\times$ 211.63 g

Sr   =   0.3810 g

Calculation of Co(NO$_3$)$_2$.6H$_2$O

LSCA6491   1 mol   =   Co 0.9 mol

LSCA6491   4.5012 $\times$ 10^{-3} mol   =   0.9 $\times$ 4.5012 $\times$ 10^{-3} mol

=   4.0511 $\times$ 10^{-3} $\times$ 291.03 g

Co   =   1.1790 g

Calculation of $Al(NO_3)_3.9H_2O$

LSCA6491	1 mol	=	Al 0.1 mol
LSCA6491	4.5012×10^{-3} mol	=	$0.1 \times 4.5012 \times 10^{-3}$ mol
		=	$4.5012 \times 10^{-4} \times 387.5$ g
Al		=	0.1744 g

Citric acid

General formula of perovskite is ABO_3, calculation based on 4.5012×10^{-3} mole LSCA 6491

To form the complex, moles of metal : moles of citric acid = 1:2

In $La(NO_3)_3.6H_2O$, the amount of metal $[NO_3]$ = 3 mole

For 2.7007×10^{-3} mole of $La(NO_3)_3.6H_2O$ $\quad \dfrac{3 \text{ mole} \times 2.7007 \times 10^{-3} \text{mole}}{1 \text{ mole}}$

$\qquad\qquad\qquad\qquad = 8.1021 \times 10^{-3}$ mole

In $Sr(NO_3)_2$, the amount of metal $[NO_3]$ = 2 mole

For 1.800×10^{-3} mole of $Sr(NO_3)_2$ $\quad \dfrac{2 \text{ mole} \times 1.800 \times 10^{-3} \text{mole}}{1 \text{ mole}}$

$\qquad\qquad\qquad\qquad = 3.6000 \times 10^{-3}$ mole

In $Co(NO_3)_2.6H_2O$, the amount of metal $[NO_3]$ = 2 mole

For 4.0511×10^{-3} mole of $Sr(NO_3)_2$ $\quad \dfrac{2 \text{ mole} \times 4.0511 \times 10^{-3} \text{mole}}{1 \text{ mole}}$

$\qquad\qquad\qquad\qquad = 8.1022 \times 10^{-3}$ mole

In $Al(NO_3)_3.9H_2O$, the amount of metal $[NO_3]$ = 3 mole

For 4.5012×10^{-4} mole of $Sr(NO_3)_2$ $\quad \dfrac{3 \text{ mole} \times 4.5012 \times 10^{-4} \text{mole}}{1 \text{ mole}}$

$\qquad\qquad\qquad\qquad = 1.3504 \times 10^{-3}$ mole

Total amount of $[NO_3]$ = $(8.1021 + 3.6000 + 8.1022 + 1.3504) \times 10^{-3}$ mole

$\qquad\qquad\qquad = 0.0212$ mole

Weight of citric acid $\quad = \quad$ 2n $\times$ MW

$\qquad\qquad\qquad\qquad = \quad$ 2 $\times$ 0.0212 $\times$ 192.13

$\qquad\qquad\qquad\qquad = \quad$ 8.1463 g

2. K_2NiF_4 –typed structure

<u>Example</u> Preparation of 1 g $LaSrCo_{0.9}Al_{0.1}O_{4-\delta}$

Molecular weight of $LaSrCo_{0.9}Al_{0.1}O_{4-\delta} = 346.27$ g/mol

$\qquad$ $LaSrCo_{0.9}Al_{0.1}O_{4-\delta}$ $\qquad$ 346.27 g $\qquad$ = 1 mol

$\qquad$ $LaSrCo_{0.9}Al_{0.1}O_{4-\delta}$ $\qquad\qquad$ 1 g $\qquad$ = 1 g/346.27 g

$\qquad\qquad\qquad\qquad\qquad\qquad\qquad\qquad$ = 2.8880×10^{-3} mol

Calculation of $La(NO_3)_3.6H_2O$

$\qquad$ $LaSrCo_{0.9}Al_{0.1}O_{4-\delta}$ $\qquad$ 1 mol $\qquad$ = $\qquad$ La 1 mol

$\qquad$ $LaSrCo_{0.9}Al_{0.1}O_{4-\delta}$ $\quad$ 2.8880×10^{-3} mol = $\qquad$ $1 \times 2.8880 \times 10^{-3}$ mol

$\qquad\qquad\qquad\qquad\qquad\qquad\qquad\qquad$ = $\qquad$ $2.8880 \times 10^{-3} \times 433.03$ g

$\qquad\qquad\qquad\qquad\qquad\qquad$ La $\quad$ = $\qquad$ 1.2505 g

Calculation of $Sr(NO_3)_2$

$\qquad$ $LaSrCo_{0.9}Al_{0.1}O_{4-\delta}$ $\qquad$ 1 mol $\qquad$ = $\qquad$ Sr 1 mol

$\qquad$ $LaSrCo_{0.9}Al_{0.1}O_{4-\delta}$ $\quad$ 2.8880×10^{-3} mol = $\qquad$ $1 \times 2.8880 \times 10^{-3}$ mol

$\qquad\qquad\qquad\qquad\qquad\qquad\qquad\qquad$ = $\qquad$ $2.8880 \times 10^{-3} \times 211.63$ g

$\qquad\qquad\qquad\qquad\qquad\qquad$ Sr $\quad$ = $\qquad$ 0.6112 g

Calculation of $Co(NO_3)_2.6H_2O$

$\qquad$ $LaSrCo_{0.9}Al_{0.1}O_{4-\delta}$ $\qquad$ 1 mol $\qquad$ = $\qquad$ Co 0.9 mol

$\qquad$ $LaSrCo_{0.9}Al_{0.1}O_{4-\delta}$ $\quad$ 2.8880×10^{-3} mol = $\qquad$ $0.9 \times 2.8880 \times 10^{-3}$ mol

$\qquad\qquad\qquad\qquad\qquad\qquad\qquad\qquad$ = $\qquad$ $2.5992 \times 10^{-3} \times 291.03$ g

$\qquad\qquad\qquad\qquad\qquad\qquad$ Co $\quad$ = $\qquad$ 0.7564 g

Calculation of $Al(NO_3)_3.9H_2O$

$\qquad$ $LaSrCo_{0.9}Al_{0.1}O_{4-\delta}$ $\qquad$ 1 mol $\qquad$ = $\qquad$ Al 0.1 mol

$\qquad$ $LaSrCo_{0.9}Al_{0.1}O_{4-\delta}$ $\quad$ 2.8880×10^{-3} mol = $\qquad$ $0.1 \times 2.8880 \times 10^{-3}$ mol

$\qquad\qquad\qquad\qquad\qquad\qquad\qquad\qquad$ = $\qquad$ $2.8880 \times 10^{-4} \times 387.5$ g

$\qquad\qquad\qquad\qquad\qquad\qquad$ Al $\quad$ = $\qquad$ 0.1119 g

Citric acid

General formula of K_2NiF_4-typed structure is A_2BO_4, calculation base on 2.8880×10^{-3} mole $LaSrCo_{0.9}Al_{0.1}O_{4-\delta}$

To form the complex, moles of metal : moles of citric acid $= 1:1$

In $La(NO_3)_3.6H_2O$, the amount of metal $[NO_3]$ = 3 mole

For 2.8880×10^{-3} mole of $La(NO_3)_3.6H_2O$ $\qquad \dfrac{3 \text{ mole} \times 2.8880 \times 10^{-3}\text{mole}}{1 \text{ mole}}$

$\qquad\qquad = 8.6639 \times 10^{-3}$ mole

In $Sr(NO_3)_2$, the amount of metal $[NO_3]$ = 2 mole

For 2.8880×10^{-3} mole of $Sr(NO_3)_2$ $\qquad \dfrac{2 \text{ mole} \times 2.8880 \times 10^{-3}\text{mole}}{1 \text{ mole}}$

$\qquad\qquad = 5.7759 \times 10^{-3}$ mole

In $Co(NO_3)_2.6H_2O$, the amount of metal $[NO_3]$ = 2 mole

For 2.5992×10^{-3} mole of $Sr(NO_3)_2$ $\qquad \dfrac{2 \text{ mole} \times 2.5992 \times 10^{-3}\text{mole}}{1 \text{ mole}}$

$\qquad\qquad = 5.1984 \times 10^{-3}$ mole

In $Al(NO_3)_3.9H_2O$, the amount of metal $[NO_3]$ = 3 mole

For 2.8880×10^{-4} mole of $Sr(NO_3)_2$ $\qquad \dfrac{3 \text{ mole} \times 2.8880 \times 10^{-4}\text{mole}}{1 \text{ mole}}$

$\qquad\qquad = 0.8664 \times 10^{-3}$ mole

Total amount of $[NO_3]$ = $(8.6639 + 5.7759 + 5.1984 + 0.8664) \times 10^{-3}$ mole

$\qquad\qquad = 0.0205$ mole

Weight of citric acid = $n \times MW$

$\qquad\qquad = 0.0205 \times 192.13 = 3.9395$ g

3. **The calculate lattice parameters**

Bragg's Law $n\lambda = 2d \sin \theta$

Cubic
$$\frac{1}{d^2} = \frac{h^2 + k^2 + l^2}{a^2}$$

Tetragonal
$$\frac{1}{d^2} = \frac{h^2 + k^2}{a^2} + \frac{l^2}{c^2}$$

Orthorhombic
$$\frac{1}{d^2} = \frac{h^2}{a^2} + \frac{k^2}{b^2} + \frac{l^2}{c^2}$$

Hexagonal
$$\frac{1}{d^2} = \frac{4}{3}\left(\frac{h^2 + hk + k^2}{a^2}\right) + \frac{l^2}{c^2}$$

Monoclinic
$$\frac{1}{d^2} = \frac{1}{\sin^2 \beta}\left(\frac{h^2}{a^2} + \frac{k^2 \sin^2 \beta}{b^2} + \frac{l^2}{c^2} - \frac{2hl\cos\beta}{ac}\right)$$

Triclinic
$$\frac{1}{d^2} = \frac{1}{V^2}\left(\begin{array}{l} h^2b^2c^2 \sin^2 \alpha + k^2a^2c^2 \sin^2 \beta + l^2a^2b^2 \sin^2 \gamma \\ + 2hkabc^2(\cos\alpha\cos\beta - \cos\gamma) \\ + 2kla^2bc(\cos\beta\cos\gamma - \cos\alpha) \\ + 2hlab^2c(\cos\alpha\cos\gamma - \cos\beta) \end{array}\right)$$

$$V = abc\left(1 - \cos^2 \alpha - \cos^2 \beta - \cos^2 \gamma + 2\cos\alpha\cos\beta\cos\gamma\right)^{1/2}$$

VITAE

Miss Paijittree Wannapak was born on March 7, 1985 in Nakhonratchasima, Thailand. She received Bachelor's Degree of Science in Industrial Chemistry from King Mongkut's University of Technology North Bangkok in 2007. Since then, she attended the Master's Degree Program of Petrochemistry and Polymer Science at Facuty of Science, Chulalongkorn University and finished her study in 2010.

Presentation

21 – 23 November 2009

Poster presentation "Chemical compatibility of new lanthanum strontium cobalt aluminium oxides and yttria stabilized zirconia" The 6th International Symposium on Advanced Material in Asia Pacific Rims, Chulalongkorn University, Bangkok.

Her present address is 17/3 Talookdoo, Thapthan, Uthaithani, 61120, Thailand. Tel 086-7125543, 056-541161, E-mail: paijittree_w@hotmail.com.